

SANDIA REPORT

SAND99-1853
Unlimited Release
Printed July 1999

Development of Zinc/Bromine Batteries for Load-Leveling Applications: Phase 1 Final Report

Phillip Eidler
Johnson Controls Battery Group, Inc.
Advanced Battery Research
5757 North Green Bay Avenue
P.O. Box 591
Milwaukee, WI 53201-0591

Prepared by
Sandia National Laboratories
Albuquerque, New Mexico 87185 and Livermore, California 94550

Sandia is a multiprogram laboratory operated by Sandia Corporation,
a Lockheed Martin Company, for the United States Department of
Energy under Contract DE-AC04-94AL85000.

Approved for public release; further dissemination unlimited.



Sandia National Laboratories

Issued by Sandia National Laboratories, operated for the United States Department of Energy by Sandia Corporation.

NOTICE: This report was prepared as an account of work sponsored by an agency of the United States Government. Neither the United States Government, nor any agency thereof, nor any of their employees, nor any of their contractors, subcontractors, or their employees, make any warranty, express or implied, or assume any legal liability or responsibility for the accuracy, completeness, or usefulness of any information, apparatus, product, or process disclosed, or represent that its use would not infringe privately owned rights. Reference herein to any specific commercial product, process, or service by trade name, trademark, manufacturer, or otherwise, does not necessarily constitute or imply its endorsement, recommendation, or favoring by the United States Government, any agency thereof, or any of their contractors or subcontractors. The views and opinions expressed herein do not necessarily state or reflect those of the United States Government, any agency thereof, or any of their contractors.

Printed in the United States of America. This report has been reproduced directly from the best available copy.

Available to DOE and DOE contractors from
Office of Scientific and Technical Information
P.O. Box 62
Oak Ridge, TN 37831

Prices available from (703) 605-6000
Web site: <http://www.ntis.gov/ordering.htm>

Available to the public from
National Technical Information Service
U.S. Department of Commerce
5285 Port Royal Rd
Springfield, VA 22161

NTIS price codes
Printed copy: A05
Microfiche copy: A01



SAND99-1853
Unlimited Release
Printed July 1999

Development of Zinc/Bromine Batteries for Load-Leveling Applications: Phase 1 Final Report

Phillip Eidler
Johnson Controls Battery Group, Inc.
Advanced Battery Research
5757 North Green Bay Avenue
P.O. Box 591
Milwaukee, WI 53201-0591

Sandia Contract No. 40-8965

Abstract

Phase 1 of the Zinc/Bromine Load-leveling Development contract (No. 40-8965) advanced zinc/bromine battery technology demonstrates that it would be appropriate for electric utilities to establish stationary energy-storage facilities. Performances of 8-cell and 100-cell laboratory batteries met or exceeded criteria that were established to address concerns observed in previous development efforts. A battery stack that remained leak free was assembled. This report details the results of the Phase 1 efforts. A leak-free battery stack was developed, and a solid technology base for larger battery designs was established. Also, using a proprietary model from Johnson Controls Battery Group, Inc., modeling to improve the integrity and performance of battery stacks was performed.

Intentionally Left Blank

Contents

Executive Summary	ix
1. Introduction.....	1-1
2. Advances in Core Technology.....	2-1
Welding Study.....	2-1
Vibration Welding Process.....	2-1
Finite Element Analysis Modeling.....	2-1
Weld Burst Tests	2-1
Materials.....	2-2
Electrodes	2-2
Experimental Separator	2-2
Glass-fiber-filled Polyethylene for Frames	2-4
Mass and Energy Balance Spreadsheet	2-4
Modeling	2-5
Battery Test Simulation	2-5
New Battery Design Optimization.....	2-14
Safety Study	2-16
Adhesive Bonding.....	2-19
3. Other Laboratory Test Results.....	3-1
Miniature Cell Tests	3-1
Current Density Studies	3-1
Separator Testing.....	3-1
Zinc Plating	3-3
Testing Methods	3-3
Zinc Loading and Current Density.....	3-3
ESCA Surface Studies	3-3
Bromine Electrode.....	3-6
Background.....	3-6
Electrochemical Surface Area.....	3-6
Optimization of Surface Chemistry	3-7
Electrolyte Composition.....	3-11
4. Battery/Station Design.....	4-1
Cooling.....	4-1
Pump/Motor Procurement	4-1
5. Laboratory Battery Cycling Results.....	5-1
Battery Cell Stacks	5-1
Production	5-1
Cycle Life	5-1
Efficiency.....	5-1
Large Cell Stacks.....	5-4
No-strip Cycling	5-4
Stand Tests	5-7
Zinc Loading	5-10
Temperature Effect.....	5-10
Fast-strip Cycling	5-10
Experimental Separator Battery Test.....	5-12
Shunt-current Protection.....	5-12
Shunt-current Protection Current.....	5-12
Shunt Currents	5-13
6. Summary/Conclusions	6-1

Figures

Figure 2-1.	Mass and energy balance spreadsheet (SNL514).	2-6
Figure 2-2.	Model voltage profile compared to an actual profile for Battery V1-53 (Cycle 3).	2-7
Figure 2-3.	Effect of electrode and separator thicknesses on energy efficiency.	2-8
Figure 2-4.	Effect of electrode resistivity on energy efficiency.	2-8
Figure 2-5.	Model-predicted voltage profile for low-resistivity electrodes compared to an actual battery cycle (V1-60, Cycle 1).	2-9
Figure 2-6.	Effect of separator resistivity on energy efficiency.	2-9
Figure 2-7.	Effect of bromine transport on energy efficiency.	2-10
Figure 2-8.	Effect of bromine transport on coulombic efficiency at 4-hour and 10-hour discharge rates.	2-11
Figure 2-9.	Effect of bromine transport and separator resistivity on energy efficiency at a 4-hour discharge rate.	2-11
Figure 2-10.	Effect of bromine transport and separator resistivity on energy efficiency at a 10-hour discharge rate.	2-12
Figure 2-11.	Effect of discharge time on efficiencies (standard 8-cell stack, no pumping losses).	2-12
Figure 2-12.	Effect of discharge time on efficiencies (standard 8-cell stack with pumping losses).	2-13
Figure 2-13.	Effect of charge time on efficiencies (zinc/bromine 8-cell stack with and without pumping losses).	2-13
Figure 2-14.	Effect of discharge time on efficiencies – Battery V1-52 versus model.	2-14
Figure 2-15.	Effect of charge and discharge times on efficiencies (80-cell system with pumping losses).	2-15
Figure 2-16.	Stand time study for Battery V1-44 compared to model predictions.	2-15
Figure 2-17.	Vapor pressures over MEPBr complex.	2-17
Figure 2-18.	Electrolyte recycling processes.	2-19
Figure 2-19.	Adhesive bonding strength.	2-21
Figure 3-1.	Effect of charge-current density on efficiencies (Minicell #2).	3-2
Figure 3-2.	Baseline cycle efficiencies (Minicell #2).	3-2
Figure 3-3.	Effect of zinc loading on dendrite height – unsupported load-leveling electrolyte (constant current density of 18 mAh/cm ²).	3-4
Figure 3-4.	Effect of current density on dendrite height (constant zinc loading of 90 mAh/cm ²).	3-4
Figure 3-5.	Effect of flow rate on dendrite height.	3-5
Figure 3-6.	Effect of flow rate on zinc thickness.	3-5
Figure 3-7.	Polarization versus cycle life for PV-2 vs. CP-4 carbon paper electrodes (data is average of >2 electrodes per run).	3-8
Figure 3-8.	ESCA-monitored changes in amorphous/graphitic carbon ratios for PV-2 carbon.	3-9
Figure 3-9.	ESCA-monitored changes in amorphous/graphitic carbon ratios for CP-4 paper carbon.	3-9
Figure 3-10.	ESCA-monitored changes in amorphous/graphitic carbon ratios for PV-2 carbon.	3-10
Figure 3-11.	ESCA-monitored changes in amorphous/graphitic carbon ratios for CP-4 carbon.	3-10
Figure 3-12.	Polarization plots, high graphite, low oxygen.	3-11
Figure 3-13.	Resistivity of ZnBr ₂ , MEPBr, and mixes versus concentration.	3-12
Figure 3-14.	Electrolyte dilution test for Battery V1-59.	3-12
Figure 5-1.	Stack V1-53 baseline cycle efficiencies.	5-2
Figure 5-2.	Stack V1-54 baseline cycle efficiencies.	5-2
Figure 5-3.	Stack V1-55 baseline cycle efficiencies.	5-3
Figure 5-4.	Stack V1-57 (SNL 518) baseline cycle efficiencies.	5-3
Figure 5-5.	Stack VL-14 baseline cycle efficiencies.	5-5
Figure 5-6.	Voltage profile of Stack VL-14 for a typical baseline cycle.	5-5
Figure 5-7.	Coulombic efficiencies for each set of no-strip cycles.	5-6
Figure 5-8.	No-strip residual amp-hour buildup.	5-7
Figure 5-9.	Battery V1-44 stand loss at full charge—watt-hour loss compared to baseline cycles.	5-9
Figure 5-10.	Battery V1-44 stand loss at full charge—amp-hour loss compared to baseline cycles.	5-9
Figure 5-11.	Zinc loading study (Battery V1-54).	5-11
Figure 5-12.	Temperature effect study—efficiency vs. operating temperature (Battery V1-50).	5-11

Tables

Table 2-1.	Burst Strength Tests	2-1
Table 2-2.	Properties of Compounded Compression-molded Separator Materials.....	2-3
Table 2-3.	Predictions from Revised Computer Model	2-5
Table 2-4.	Cell Stack Optimization	2-16
Table 2-5.	Type of Analysis.....	2-19
Table 2-6.	Adhesive Bonding Tests on Polyethylene	2-20
Table 3-1.	Separator Comparison	3-2
Table 5-1.	Summary of 8-Cell Stacks Built In Phase 1.....	5-1
Table 5-2.	Large V-Design Batteries	5-4
Table 5-3.	Averages of Sets of No-strip Cycles.....	5-6
Table 5-4.	Stand-loss Results.....	5-8
Table 5-5.	Strip Times	5-10
Table 5-6.	V1-51 Performance – Energy Losses	5-12

Intentionally Left Blank

Acronyms

A/G	amorphous/graphitic
BET	Brunauer, Emmett, and Teller
ESCA	electron spectroscopy for chemical analysis
HDPE	high-density polyethylene
ICP	inductively coupled plasma
IR	ohmic current/internal resistance
JCBGI	Johnson Controls Battery Group, Inc.
KCl	potassium chloride
MEM	methylethylmorpholinium
MEP	methylethylpyrrolidinium
MEPBr	methylethylpyrrolidinium bromide
SCP	shunt-current protection
Sd	standard deviation
SNL	Sandia National Laboratories
TGA	thermogravimetric analysis
WASP	water slurry process
ZnBr ₂	zinc bromide

Intentionally Left Blank

Executive Summary

The Zinc/Bromine Load-leveling Battery Development contract (No. 40-8965) was partitioned at the outset into two phases of equal length. Phase 1 started in September 1990 and continued through December 1991. In Phase 1, zinc/bromine battery technology was to be advanced to the point that it would be clear that the technology was viable and would be an appropriate choice for electric utilities wishing to establish stationary energy-storage facilities. Criteria were established that addressed most of the concerns that had been observed in the previous development efforts. The performances of 8-cell and 100-cell laboratory batteries demonstrated that the criteria were met or exceeded. In Phase 2, 100-kWh batteries will be built and demonstrated, and a conceptual design for a load-leveling plant will be presented. At the same time, work will continue to identify improved assembly techniques and operating conditions.

This report details the results of the efforts carried out in Phase 1. The highlights are listed below.

- Four 1-kWh stacks achieved over 100 cycles.
One 1-kWh stack achieved over 200 cycles.
One 1-kWh stack achieved over 300 cycles.
- Less than 10% degradation in performance occurred in the four stacks that achieved over 100 cycles.
- The battery used for the zinc loading investigation exhibited virtually no loss in performance for loadings up to 130 mAh/cm².
- Charge-current densities of 50 ma/cm² have been achieved in minicells.
- Fourteen consecutive no-strip cycles have been conducted on the stack with 300+ cycles.
- A mass and energy balance spreadsheet that describes battery operation was completed.
- Materials research has continued to provide improvements in the electrode, activation layer, and separator.
- A battery made of two 50-cell stacks (15 kWh) was produced and delivered to Sandia National Laboratories (SNL) for testing.

The most critical development was the ability to assemble a battery stack that remained leak free. The task of sealing the battery stack using vibration welding has undergone significant improvement resulting in a viable production process. Through several design iterations, a solid technology base for larger battery stack designs was established. Internal stack stresses can now be modeled, in addition to fluid velocity and fluid pressure distribution, through the use of a finite element analysis computer program. Additionally, the Johnson Controls Battery Group, Inc. (JCBGI) proprietary FORTRAN model has been improved significantly, enabling accurate performance predictions. This modeling was used to improve the integrity and performance of the battery stacks, and should be instrumental in reducing the turnaround time from concept to assembly.

Intentionally Left Blank

1. Introduction

Batteries, especially lead-acid batteries, are used at present by electric utilities and various other industries for applications such as load leveling, frequency regulation, and spinning reserve. Batteries can balance electricity supply and demand, for example, by contributing power during the periods of peak usage. The batteries are later recharged during off-peak hours. Zinc/bromine batteries are attractive candidates for load-leveling applications because they offer two to three times the specific energy of lead-acid batteries, have sufficient power, operate at near room temperature, are recyclable, are low cost to build, and have the potential for long life.

The zinc/bromine battery is composed of three parts: the cell stack, the reservoirs, and the electrolyte circulation system. The electrode reactions take place in the cell stack. The battery starts each cycle with the same composition zinc-bromide ($ZnBr_2$) electrolyte in each reservoir. The two electrolytes are continuously pumped in separate circulation loops through the anode and cathode chambers in the stack. During charge, zinc is plated on the anode side of a bipolar electrode, while bromine is formed on the cathode side. The bromine instantly forms a complex with quaternary ammonium ions in the electrolyte, and this complex separates from the aqueous solution forming a second, denser liquid phase. Depleted aqueous electrolyte and the second-phase flow continuously from the stack and are replaced by fresh electrolyte from the reservoirs. The newly produced second-phase falls to the bottom of the catholyte reservoir because it is denser than the aqueous solution. The second-phase remains in the catholyte reservoir throughout the charge period. Then, during discharge, an emulsion of second-phase and aqueous solution is circulated through the cathode chamber. The bromine, complexed in the second-phase and to a lesser extent dissolved in the electrolyte, reacts at the cathode surface to form bromide ions. In the anolyte, the plated zinc metal oxidizes to form zinc ions.

The cell stack is composed of a number of bipolar electrodes and cell separators with terminal electrodes on either end. The electrodes are made from electrically conducting carbon plastic and are thermally welded into a nonconducting plastic flow frame. The flow frame contains the channels and openings used to conduct the electrolyte to and from the electrodes. The same flow-frame design is used for both elec-

trodes and separators. The flow frames are vibration-welded together to form the body of the cell stack. Rigid endblocks are placed outside the terminal electrodes to resist outward bending forces that are present when electrolyte is pumped through the stack.

The objectives of this program were to design, fabricate, evaluate, and optimize a zinc/bromine battery system suitable for utility energy storage. The approach used by Johnson Controls Battery Group, Inc. (JCBGI) was to demonstrate the suitability of the zinc/bromine battery in a design that is approximately one half the final electrode size. In this phase of the program, the test batteries would meet or surpass the performance criteria set by Sandia National Laboratories (SNL). Then, based on the experience gained from building and operating the smaller design, the final battery system would be developed for utility energy storage in Phase 2. It is anticipated that the production of a battery with larger-size electrodes will require a complete new set of plastic injection molds and tooling. Because this is time consuming and relatively expensive, a lot of time and attention was devoted to the design to ensure that it will need to be done only once.

Phase 1 of the program met several criteria proposed by SNL to demonstrate the soundness of the technology. These criteria were:

1. Demonstrate leak-free battery stacks.
2. Demonstrate steady long-term operation by achieving more than 100 cycles with less than a 10% drop in energy efficiency.
3. Achieve energy efficiencies in the range of 75%.
4. Demonstrate adequate performance with six consecutive no-strip cycles.
5. Attain an eventual battery cost target of \$150/kWh or less.
6. Address safety issues associated with the battery.

This report describes how most of these criteria were met or exceeded, and discusses further work that was done on improving the battery materials, the assembly processes, and the ability to recycle the batteries.

To verify the zinc/bromine battery design, several batteries were delivered to SNL for testing. An 8-cell state-of-the-art battery station was delivered at the

beginning of the project, and a twin, 50-cell-stack, improved state-of-the-art station was delivered early in February 1992. This new battery included most of

the technology improvements made so far, and it demonstrated the capabilities of zinc/bromine batteries for load-leveling operation.

2. Advances in Core Technology

Welding Study

Vibration Welding Process

The literature was searched on how to improve the vibration welding process. This literature showed that little is known at this time, and we would have to proceed with an empirical study. In such a study, a “window of operation” is determined by varying the process parameters.

A major parameter in the vibration welding process is the composition of the plastic. Various melt index polyethylene-glass-content levels, along with part dimensions, were studied in a welding test using small coupons. These welded coupons were then tested for strength and results used to set up the parameters on the full-size parts.

Finite Element Analysis Modeling

A finite element analysis computer program was used for frame design modeling. The cell-stack frames were analyzed for stresses when pressurized to find out where the highest stresses would occur, and what the magnitudes of the stresses would be at those locations.

Symmetry was used to reduce the size of the model, and still obtain accurate results. Only one quarter of a flow frame was needed in the model. For modeling the contact area stresses in normal operation, a 10-psi electrolyte pressure was simulated. The model indicated that the highest stress is located at the center of the stack. In actual battery-stack burst tests, the stacks failed at an internal pressure of 26 psi (discussed below). The equivalent stress where the stacks failed as predicted by the model was within about 4 percent of the measured failure stress in test coupons of the same material.

Calculations done for the final large-size electrode showed that it would have about the same stress at 26 psi as the test-cell stack, which should provide a similar safety factor.

When analyzing the flow distribution over the current frame, the model predicted a flow similar to the flow

that was seen in videotaped flow tests. The diverter pattern was then changed for improved, more uniform flow.

In the new flow-frame design, finite element analysis will reduce the design time by balancing the flow before cutting the mold, and ensure a properly-sized weld.

Weld Burst Tests

Several stacks were pressurized with air to determine the failure pressure and location of the failure points. The stacks were built by welding four flow frames between standard endblocks. Table 2-1 summarizes the tests, failure points, and failure pressures. The modified parts refer to strengthening done at a specific point by adding more plastic; either like the original or virgin high-density polyethylene (HDPE). Item 2 in Table 2-1 was modified with the original plastic in the weld. Item 3 was modified using HDPE. In some cases, the welds failed; in other cases, the stack material broke.

Table 2-1. Burst Strength Tests

Test	Failure Point	Pressure
1. Pre-study parts	Interior frame	17 psi
2. Modified - w/like original weld	Endblock cover weld	21 psi
3. Modified - w/HDPE	Endblock cover weld	26 psi
4. Standard build	Endblock material	26 psi
5. Standard build	Frame material and welds	26 psi

The test results indicate that the stacks can withstand a pressure of 26 psi before failure. Because the batteries are operated at design pressure of 10 psi, this gives a safety factor of 2.6.

Materials

Electrodes

Extruded Carbon Plastic

A series of carbon-plastic materials were prepared by a vendor during August of 1990 in an effort to maximize the conductivity and to minimize their expansion in bromine. The type of plastic, type of carbon, and compounding parameters were varied. None of the compositions contained glass-fiber reinforcing. The results showed a large range of conductivity, from 3 to 22 (ohm-cm)⁻¹, and a small range in expansion, 1.9 to 3.6% after 24 hours in bromine vapor.

The results of this study showed that formulations could be made with substantially lower resistivities than those of typical extruded glass-fiber-filled conductive plastics. However, the usefulness of these formulations is limited because at this time, state-of-the-art extruded materials require glass fiber to resist bromine-induced expansion.

In March 1991, another set of carbon-plastic compositions was compounded, this time with glass fiber. Two series of compositions were made. Both series used 16 wt% glass fiber, but used different carbons. It was found that while the lowest resistivities were achieved with high loadings of carbon, this was done at the expense of tensile strength. Bromine expansion tests took 24 hours, and the samples did not expand appreciably when given more time. All of the results were in the range of 1.0 to 1.5%, which was smaller than the samples without glass fiber.

One problem with these electrodes is the high incidence of small lumps in the trimmed sheets. These lumps are usually about 1/8 in. diameter. They are hard and sometimes protrude so they are slightly thicker than the rest of the sheet. The lumps were analyzed, but the results were inconclusive. In future production runs, samples of the unextruded compound will be compression molded to determine whether the lumps are inherent in the compounded material, or whether they are a result of the extrusion process.

Water Slurry Process Electrodes

In addition to producing carbon-plastic electrode sheets by extrusion, they can be made by a process similar to paper-making called the water slurry process (WASP). In this process, small pieces of com-

pounded carbon plastic are mixed with glass fibers and filtered into a felt mat. The mat is then heat-pressed into a dense, impervious sheet. The key difference from extruded materials is that the carbon plastic is randomly oriented so it should expand less in the X-Y dimensions.

Battery V1-42 was made with the WASP electrodes. It was torn down at 47 cycles because it seeped electrolyte at the anode studs. The electrodes were found to be slightly warped. The warpage did not appear quite as extensive as with extruded electrodes, but was greater than expected, based on earlier accelerated tests of coupons in bromine vapor. Additionally, the zinc plating was spotty in places, which suggested porosity, or the disruption of plating by large concentrations of glass fiber just under the surface.

A general problem with water slurry electrodes is that the consolidation process used by the manufacturer uses only very light pressure (around 30 psi). It is expected that the final user will further press and consolidate the material. Also, unless the plastic has a very low viscosity, the final consolidated product tends to be porous. Full densification thus requires a secondary batch process (heat-pressing in a very large hydraulic press), which adds considerably to the cost.

Experimental Separator

Vendor-produced Materials

Samples of separator materials were produced by extrusion and by compression molding. The major focus of the tests was to examine the effect of silica loading.

When equipment problems at the vendor's factory forced the postponement of a pilot-line production run of zinc/bromine separator, the material was prepared on their 48-inch-wide production line. While waiting for the large-size production run, small batches of separator composition were compounded in their Brabender torque rheometer to continue their development program. These were then compression molded to produce 0.025-inch sheets, which could then be tested. Little or no difference in properties could be determined between extruded and compression-molded sheets having the same composition. An advantage of producing samples in this manner is that it is less expensive per sample than producing them by extrusion.

Several small (50-70 g) batches of polyethylene-based separator compositions were produced this way. Table 2-2 shows the test results of these samples. These were the first results using the new load-leveling electrolyte. With this electrolyte, bromine-transport measurements tend to be lower, and resistivity measurements tend to be higher than with electric vehicle electrolyte. Asahi SF-600 and "standard" extruded zinc/bromine separator properties are compared to those of prepared samples.

The most important finding from these tests was that the bromine transport for the new material was much higher than expected. At first it was not clear whether this was caused at least in part by the different electrolyte used for the test, because earlier runs of extruded separator had properties that were closer to those of the Asahi material. On further investigation, the vendor divulged that the type of one material had been changed from previous extrusion runs. They explained that the two types had been used somewhat interchangeably in their commercial product, and that there were few detectable differences in the properties of the two materials. So while this may be a factor, it is probably not that the entire cause of the high-transport problem. Another possible factor was that ash-test results showed that the silica level was slightly off the specification. Further aspects of the problem may relate to the slight differences between the pilot-line equipment and the production equipment.

A further set of experiments was again done by compounding and compression molding, rather than by extrusion. This series was designed to systematically investigate the effects of the silica-to-plastic ratio and different types of polyethylene.

It was found that higher silica loadings gave lower resistivity in all cases. One kind of polyethylene plastic had the best bromine transport with high loadings of silica. However, the samples were extremely weak and almost certainly would prove impossible to extrude. These results validate the previous approach of using blends of two different polyethylene plastics in extruded separator.

Future work will explore the use of other types of silica, and possibly some further investigations will be done using polymers other than polyethylene.

Ion-exchange Coatings for Separators

Several pieces of 10.5 × 12-inch experimental and Asahi SF-600 separator were sent to SNL for coating with fluorinated cation-selective resin and other ion-exchange resins. The separator sheets sent to SNL were of a size large enough for testing in the JCBGI minicells.

The coated SF-600 samples received from SNL were tested for bromine transport. The result was 1.26 and 1.29×10^{-9} mol/cm² sec. For untreated SF-600 the measurement was 3.37×10^{-9} . However, the increase in resistivity as measured by JCBGI was of the same magnitude. An additional problem was that the coated separators could no longer be welded into polyethylene frames. A method was worked out to allow the coated separators to be tested in cells without having to weld them.

The standard separator treated with a similar type of ion-exchange resin from a second vendor fared somewhat better. The treatment increased the resistivity by only 17%, while it decreased the bromine

Table 2-2. Properties of Compounded Compression-molded Separator Materials

Separator Material	Thickness (mm)	Resistivity (ohm-cm)	Br ₂ Flux * 10 ⁻⁹ (mole/sec-cm ²)
Asahi SF-600	0.60	1.28	3.3
Advanced Zn/Br electric vehicle (extruded)	0.61	0.75	6.0
Compression molded, T ₁	0.40	0.67	6.4
Compression molded, T ₂	0.40	0.68	7.1
Compression molded, T ₃	0.46	0.66	6.8

transport by 43%. When this material was tested in a minicell, it gave an improvement in coulombic efficiency of about 2% and a slight decline in voltaic efficiency. The net result was an energy efficiency improvement of about 1%. This is a small but significant improvement. It may prove to be more significant under different cycle conditions, for example, slower charge/discharge rates and/or long stand times.

Self-discharge Current Equivalent to Bromine Transport

The transport of bromine across the separator is the primary mechanism of self-discharge. This rate can be measured in an independent test by placing a well-mixed standard solution of bromine and electrolyte on one side of a separator with the same solution but no bromine on the other side. The transport rate is found by analyzing the increase in bromine concentration on the other side. This, in turn, can be stated in terms of a pseudo-current. The calculation for a V-design laboratory cell (Asahi SF-600 separator and load-leveling electrolyte) is as follows:

The measured transport rate is ...

$$3.4 \times 10^{-9} \text{ mol Br}_2/\text{cm}^2\text{-sec} \times \\ (1175 \text{ cm}^2) (3600 \text{ sec/hr}) (2 \text{ equiv./mol Br}_2) (26.8 \text{ Ah/equiv.}) \\ = 0.77 \text{ A.}$$

Thus 0.77 A is the equivalent self-discharge current resulting from bromine diffusion across the separator.

The self-discharge rate can be taken as the transport loss portion of the coulombic inefficiency. This is calculated in the JCBGI spreadsheet (discussed below) and the agreement with the transport rate derived current is fairly good. The self-discharge rate calculated for a baseline cycle is 0.824 A.

Glass-fiber-filled Polyethylene for Frames

The chopped glass fibers and polyethylene plastic used in the extruded electrodes and injection-molded frames were exposed to electrolyte with and without second-phase bromine complex, and a surface effect was observed. To test the fibers, they were initially dried for two hours at 250°F, weighed to three decimal places, and immersed in the two solutions for one week at room temperature. Then the fibers were filtered and rinsed thoroughly with distilled water. Finally the fibers were dried at 250°F and weighed after two hours and again after four hours of drying.

In the case of standard load-leveling electrolyte, the weight increased by 2.4% after immersion for one week. These fibers were also noticeably a darker yellow color than the original fibers. The weight of the fibers immersed in the second-phase catholyte solution increased 1.9% after one week, and the color changed from a light yellow to a grey-brown color. The weight of the fibers in each case was essentially the same after four hours as it was after two hours, indicating that the fibers were thoroughly dried after four hours.

The glass fibers were analyzed by energy-dispersive x-ray to determine the elemental makeup of the surface. Both zinc and bromine were found on the surface of the tested fibers, but none was found on the surface of the untreated fibers. The fibers immersed in load-leveling electrolyte contained 0.81 atom percent zinc and 1.47 atom percent bromine, while the fibers treated with second-phase catholyte had 0.61 atom percent zinc and 1.75 atom percent bromine. These results indicate that zinc bromide electrolyte alters the surface of the glass fibers, but the effect this has on actual battery component properties is not known.

Several pieces of frame material were exposed to second-phase catholyte and pure polybromide complex phase for one week and compared to the virgin material using ESCA. Surface studies indicate significant decreases in the silicon and oxygen contents at the surface, which suggests degradation of the silane-coupling agent used in processing the fibers. Also the bromine appears to have reacted with some of the carbon atoms at the interface. The carbon could be from the HDPE, the silane coupling agent, or an organic binder used on the glass fibers. Similar results were confirmed using Fourier Transform Infrared Spectroscopy (FTIR) and thermogravimetric analysis (TGA) to examine the bulk material. Bromine reacting with silanes and binders at the glass/HDPE interface, weakens the bulk-frame material.

Mass and Energy Balance Spreadsheet

A computer spreadsheet was written that describes some of the mass balance and energy losses of test batteries. The spreadsheet does not predict energy losses, but shows which factors account for the measured loss. The value of the spreadsheet is that it can calculate how much of the electrolyte is being utilized

(important information when chloride salts are substituted for bromide), and the various trade-offs between diffusion losses and resistance losses can be clearly shown.

A copy of the spreadsheet written for the Battery SNL514 is shown in Figure 2-1. The data entered consists of the volume and concentration of the electrolyte, the amp-hour and watt-hour readings from a typical cycle, an estimate of the overvoltage at the zinc and bromine electrodes, and an estimate of the per cell resistance. From these numbers, the utilization of the zinc, bromide, etc. are calculated, and the ratio of bromine to complexing agent is determined. The overall efficiencies are calculated and can be compared to the results of the cycle from which the data was taken. The overall average voltage on charge and discharge are calculated.

The losses caused by shunt currents are found through a multi-step process. First, the thicknesses of the electrodes and electrolyte gaps and their resistivities are used to calculate resistances in the channels and manifolds. A calculation of the expected cell resistance is also made from component resistivities and dimensions. This is compared to a measured value that is entered. If they are not relatively close to each other, the values should be checked. In a final check, the apparent resistance of the battery is found by a $\Delta V/\Delta I$ calculation. In the attached spreadsheet of Battery SNL514, the cell resistance, which was entered as 5.5 m Ω , is calculated from the resistivities as 5.1 m Ω , and is verified from the cycling results as 6.0 m Ω . A BASIC language program was supplied by SNL that calculates the shunt currents in the channels and manifolds depending on the resistances.¹ The BASIC program is run three times, once each for the different voltages on charge, open circuit, and discharge. The total current in the manifold is found by adding the current at each cell, and then the equivalent amps per cell are found by dividing by the number of cells. This value is then multiplied by four because there are four manifolds. This represents the current that bypasses the cells in the battery and is entered into the spreadsheet.

The energy losses are calculated individually, and the sum is compared to the actual measured loss. A dif-

ference of less than 10% is considered good. The energy losses are restated in terms of percent of the total. The energy lost to bromine diffusion now closely matches that predicted by the FORTRAN zinc/bromine model. However, the energy lost to shunt currents is still less than that predicted by the model. A slope of the overvoltage-free volts/amps taken from the currents and average voltages is calculated, as a check on the entered ohmic resistance. These numbers should also be in agreement.

The weakness of the spreadsheet is that it is a summary of the whole cycle. The resistance, concentration, diffusion rates, etc., change during the cycle. The spreadsheet calculations are based on the total performance during a cycle.

Modeling

Battery Test Simulation

Many improvements and changes have been incorporated into the JCBGI FORTRAN zinc/bromine computer model to better calculate voltage profiles similar to those of an actual battery. This, in turn, means that efficiencies and discharge energy predictions have become more accurate. The battery voltage profile (V1-53, Cycle 3) is compared to the original and improved models in Table 2-3 and Figure 2-2.

Table 2-3. Predictions from Revised Computer Model

	V1-53 (Cycle 3)	Original Model	Improved Model
Amp-hr in:	105.6	123.2	105.2
Watt-hr in:	1604.3	1890.5	1608.2
Disch. time:	228.7	178.6	232.3
Amp-hr out:	93.0	72.9	93.5
Watt-hr out:	1195.7	877.7	1192.7
Coulombic %:	88.1	68.2	88.9
Voltaic %:	84.6	75.0	83.4
Energy %:	74.5	51.2	74.2

¹ E. Kaminski and R. Savinell. 1983. "A Technique for Calculating Shunt Leakage and Cell Currents in Bipolar Stacks Having Divided or Undivided Cells," *J. Electrochemical Soc.* Vol. 150, p. 1103.

ZINC/BROMINE MASS AND ENERGY BALANCE

"MASSENERGYBAL4"

25 - JUL - 1991
10:30:04 AM

First order calcu
Based on SNL514/2

Inputs:			
Electrolyte:			
Volume	54.57 liter		50
ZnBr2	2.25 M	Area per cell	1170 cm2
ZnCl2	0.5 M	Anode Overvoltage	0.011 v
Quat	0.8 M	Cathode Overvoltage	0.011 V
Resistivity	14 Ohmcm	Meas. Resis./cell	5.5 mohm
Electrode C-Plastic	5.5 Ohmcm		
Separator	40 Ohmcm	Manifold Len./cell	0.301 cm
Separator	54 Ohmcm	Manifold Diameter	1.5 cm
Electrode Thickness	30 mil	Channel Length	45.7 cm
Electrode Gaps	65 mil	Channel Area	0.051 cm2
Separator Thickness	23.5 mil		
Electrode Thickness	0.076 cm	Resistance (calc)	5.1 mohm
Electrolyte Gaps	0.165 cm	R. channel	12545 Ohm
Separator Thickness	0.060 cm	R. manifold/cell	2.39 Ohn
Charge Current	23.5 Amp	Discharge Current	24.2 Amp
Charge Time	4.7 hour	Discharge Time	3.9 hour
Amp Hours in	110.6	Amp Hours out	94.7
Watt Hours in	10529.6	Watt hours out	7456.0
Stand time	0.0 hour	Strip	7.3 AmpHr
Equiv. SC Charge	0.131 Amp	Equiv. SC Discharge	0.096 Amp
		Equivalent SC Stand	0.117 Amp
Results:			
Total Zinc	150.07 Moles	Stack Efficiencies:	
Zinc Plated	103.17 Moles	Coulombic	85.62 %
Zinc Plated	94.53 mah/cm2	Voltaic	82.70 %
Zinc in Solution	46.90 Moles	Energy	70.81 %
Zinc Utilization	68.75 %	Trans	7.78 %
ZnBr2 Utilization	84.03 %	Resid	6.60 %
Total Bromide	289.22 Moles		
Bromide Available	245.57 Moles	Charge Voltage	1.9 V
Bromide remaining	39.22 Moles	Discharge Voltage	1.6 V
Bromide Utilization	84.03 %		
Total Bromine	103.17 Moles	Shunt Current	0.99 Ah
Bromine/Quat	2.36	Br2 Diffusion	3.9e-09 mol/cm2
		equil. current	0/754 mA/cm2
		Stack current	0.883 A
Resistance Losses	1344.98 Whr	Resistance Losses	44.6 %
Overvoltage Losses	225.83 Whr	Overvoltage Losses	
Shunt Curr Losses	88.33 Whr	Shunt Curr Losses	
Diffusion Losses	661.57 Whr	Diffusion Losses	21.9 %
Residual Losses	694.95 Whr	Residual Losses	23.0 %
Total	3015.66 Whr	Total	100.0 %
Actual	30.73.00 Whr		
Deviation	1.87 %	Check Value:	
		(Average volt/curr)	6.0 mohm)

Figure 2-1. Mass and energy balance spreadsheet (SNL514).

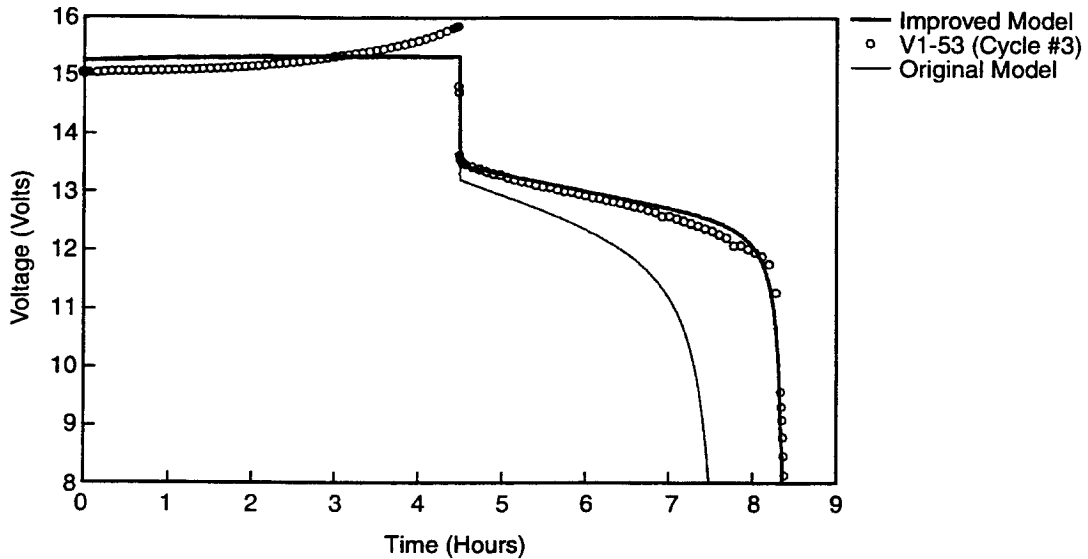


Figure 2-2. Model voltage profile compared to an actual profile for Battery V1-53 (Cycle 3).

Effect of Material Properties

Computer modeling has been used to examine the effects of trade-offs in electrode and separator material properties on zinc/bromine battery performance. Iterations were run on the model over a range of material (electrode and separator) properties and are plotted in Figures 2-3 to 2-7.

The data in Figure 2-3 indicates that decreasing electrode thickness could show a 0.5% increase in energy efficiency. The lower limit on electrode thickness would be determined by material property and warpage considerations. The separator thickness shows a peak in efficiency at 0.025 inches, caused by a trade-off between resistivity and bromine transport. The increase shown at very small separator thicknesses is caused by an assumption in the model that bromine diffusion is governed by the smaller of the separator and bulk diffusion terms, but again lower limits

would depend on the physical properties of the separator.

The model results in Figure 2-4 show that improvements of 2% in energy efficiency could be obtained by using lower resistivity electrodes. Actual improvements in energy efficiency of 1 to 2% were observed when lower resistivity electrodes were used in Batteries V1-59 and V1-60. The model-predicted voltage profile for a battery with low-resistivity electrodes is compared to an actual battery cycle in Figure 2-5. This again shows a very good correlation between the model and actual results.

Similarly, an increase of 1% could be observed by decreasing the separator resistivity as seen in Figure 2-6. A critical property of the separator appears to be the bromine transport. Significant improvements in energy efficiency could be observed by decreasing the bromine transport as shown in Figure 2-7, but this

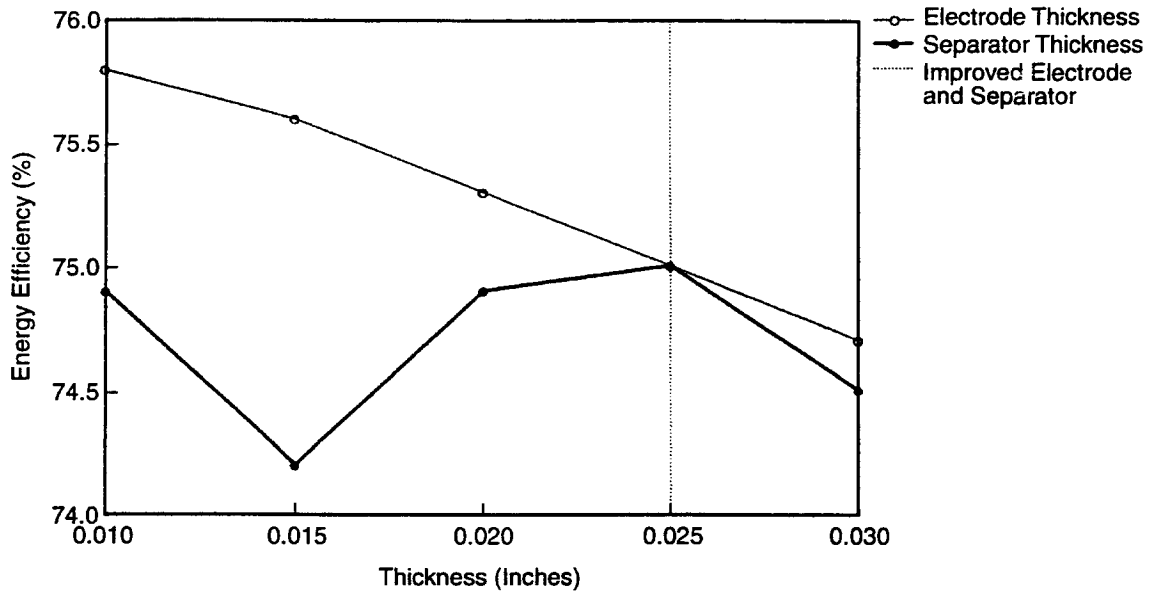


Figure 2-3. Effect of electrode and separator thicknesses on energy efficiency.

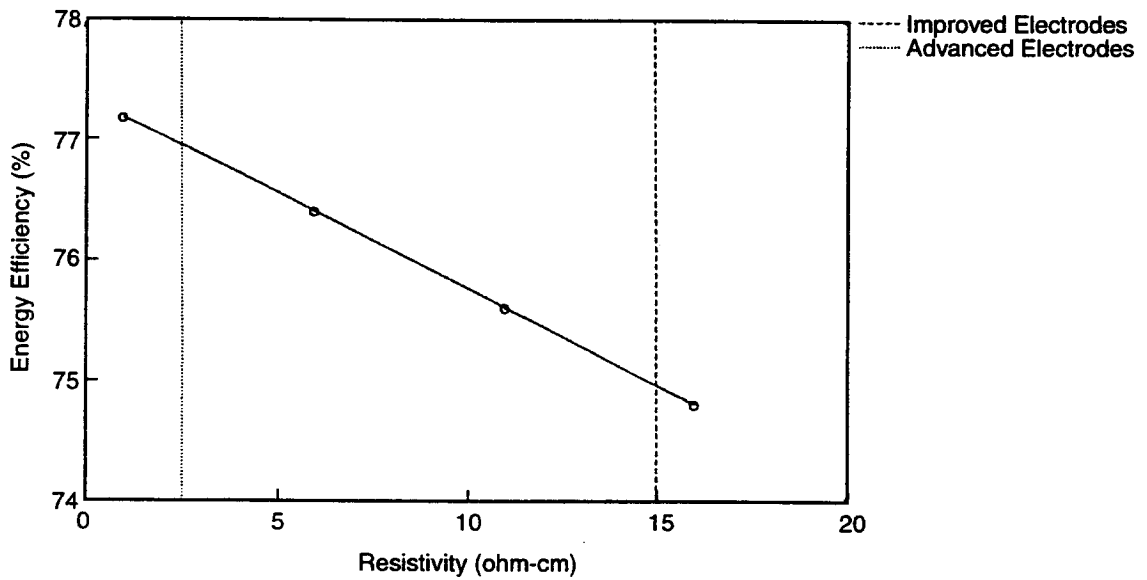


Figure 2-4. Effect of electrode resistivity on energy efficiency.

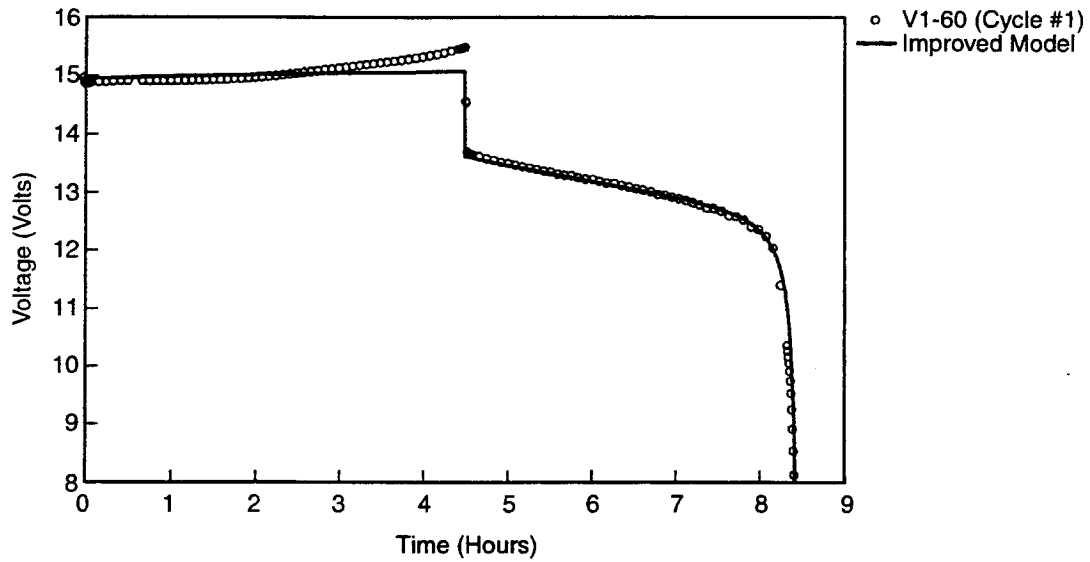


Figure 2-5. Model-predicted voltage profile for low-resistivity electrodes compared to an actual battery cycle (V1-60, Cycle 1).

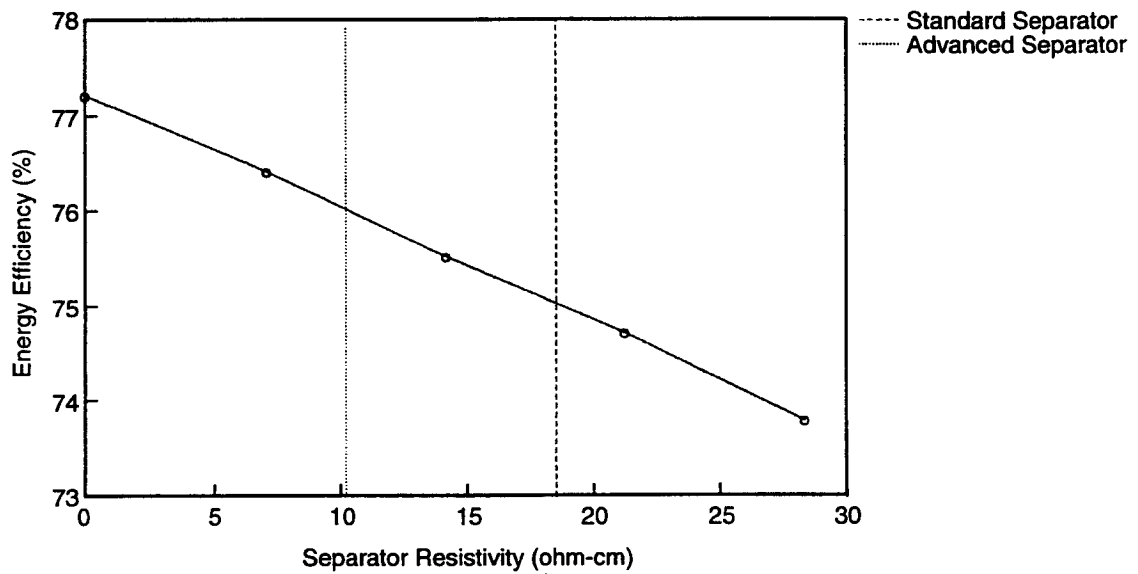


Figure 2-6. Effect of separator resistivity on energy efficiency.

is not a simple property to improve. Also, there appears to be a physical trade-off between bromine transport and separator resistivity that may need to be optimized for the best battery performance.

Effect of Discharge Rates

The computer model was used to examine the effects of bromine diffusion and separator resistivity on efficiencies for 4-hour and 10-hour discharge rates. The curves in Figure 2-8 show how coulombic efficiency is affected by bromine diffusion for both discharge rates. It can be seen that coulombic efficiency is more sensitive to bromine diffusion for the 10-hour discharge than for the 4-hour discharge, which would be expected because of the extended time available for bromine diffusion.

Figures 2-9 and 2-10 show the trade-off between bromine diffusion and separator resistivity on energy efficiency for 4-hour and 10-hour discharge rates respectively. These plots indicate that by lowering the bromine transport, a higher resistivity separator could be used to obtain the same energy efficiency. This trade-off appears to be more important at the 10-hour discharge rate than at the 4-hour rate.

The effect of length of discharge on battery stack performance can be observed in Figure 2-11 for a standard 8-cell battery. This shows that the stack energy efficiency reaches a maximum at about a 7-hour discharge, while batteries that are currently on test are run with a 4-hour discharge. It appears that a slight increase in stack energy efficiency could be obtained by going to a 6- to 8-hour discharge. When examining the entire system (including pumping losses), a shorter discharge time would be more favorable as seen in Figure 2-12. The optimum energy efficiency would be obtained with an approximately 4-hour discharge rate.

A similar analysis was performed considering the charge cycle for an 8-cell zinc/bromine battery. The effect of charge time (keeping the total zinc loading constant at 90 mAh/cm²) is seen in Figure 2-13 for an 8-cell battery with and without pumping losses. This indicates that the energy efficiency would peak at about a 7- to 8-hour charge rate when pumping losses are not included, while the peak shifts to a shorter charge time of six hours when including pumping losses.

During actual battery testing using V1-52, it was observed that residual losses are affected by discharge

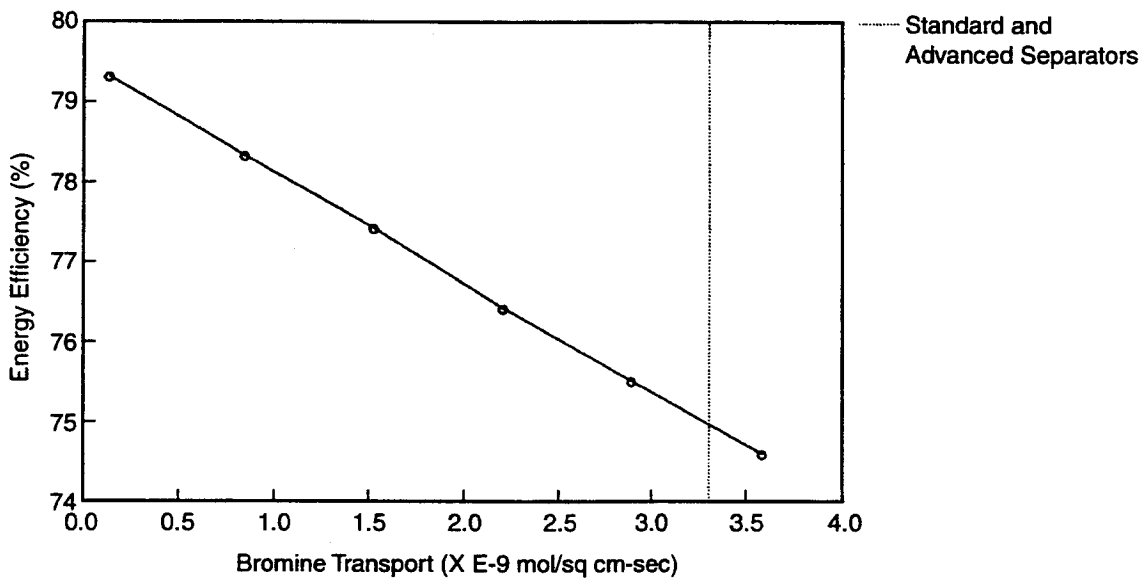


Figure 2-7. Effect of bromine transport on energy efficiency.

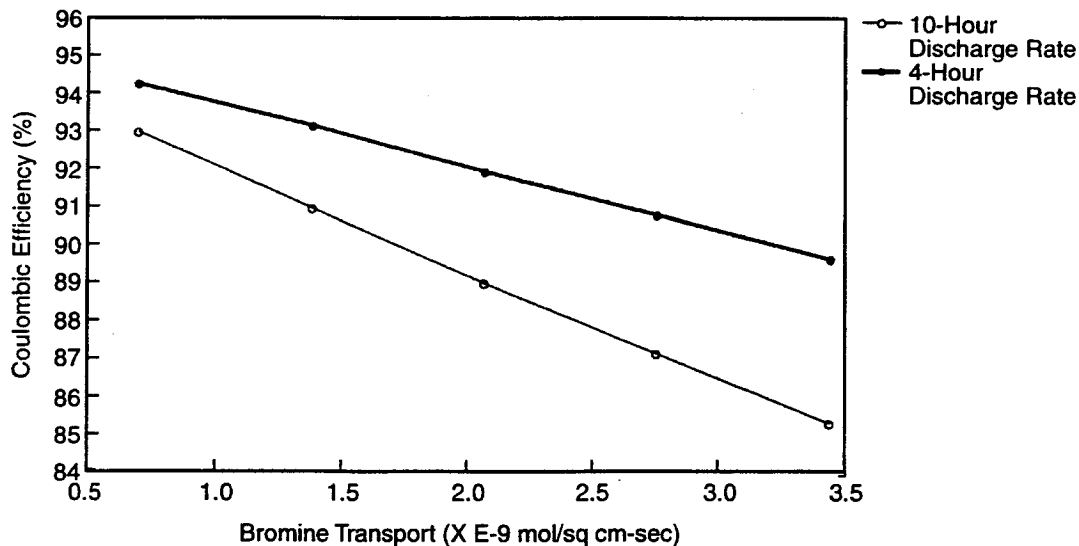


Figure 2-8. Effect of bromine transport on coulombic efficiency at 4-hour and 10-hour discharge rates.

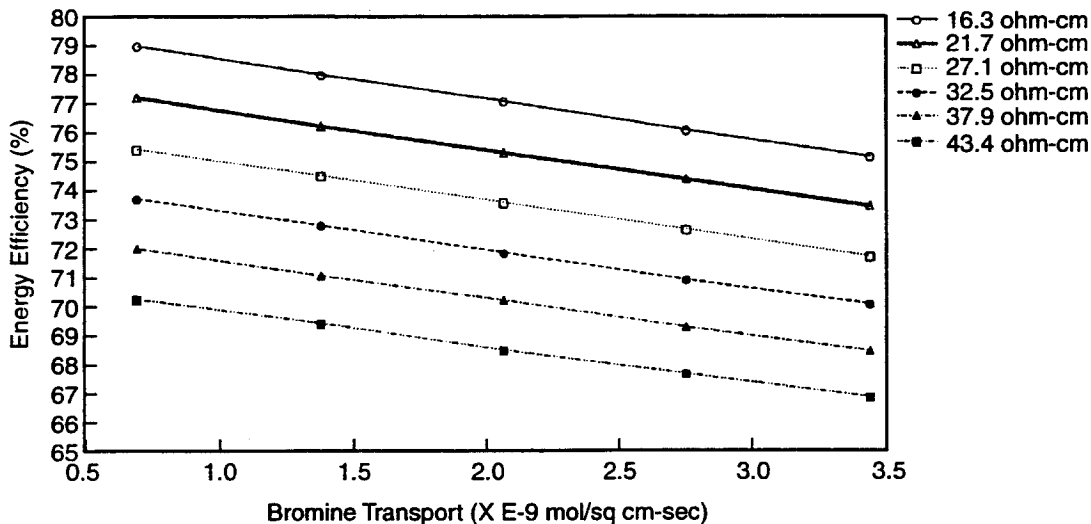


Figure 2-9. Effect of bromine transport and separator resistivity on energy efficiency at a 4-hour discharge rate.

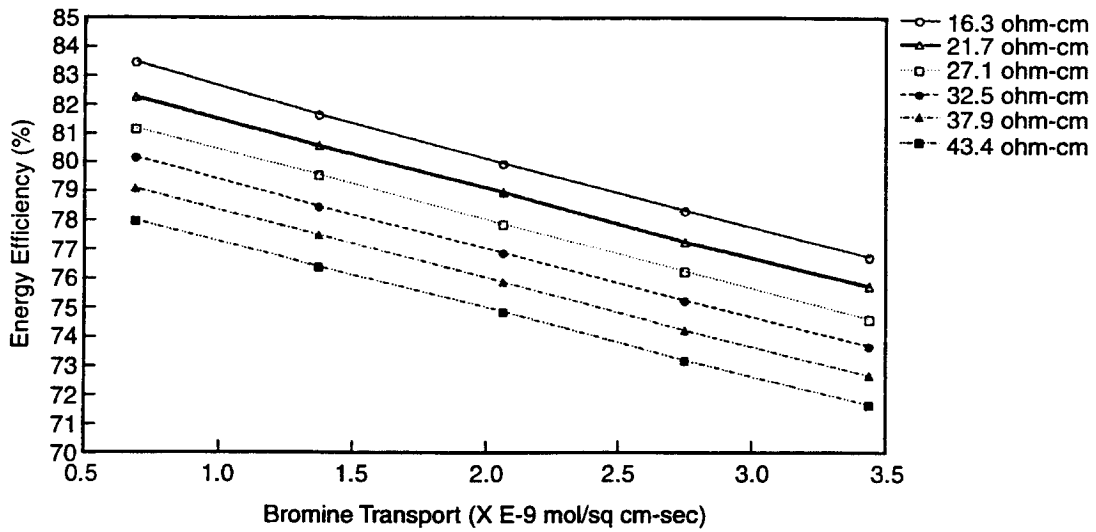


Figure 2-10. Effect of bromine transport and separator resistivity on energy efficiency at a 10-hour discharge rate.

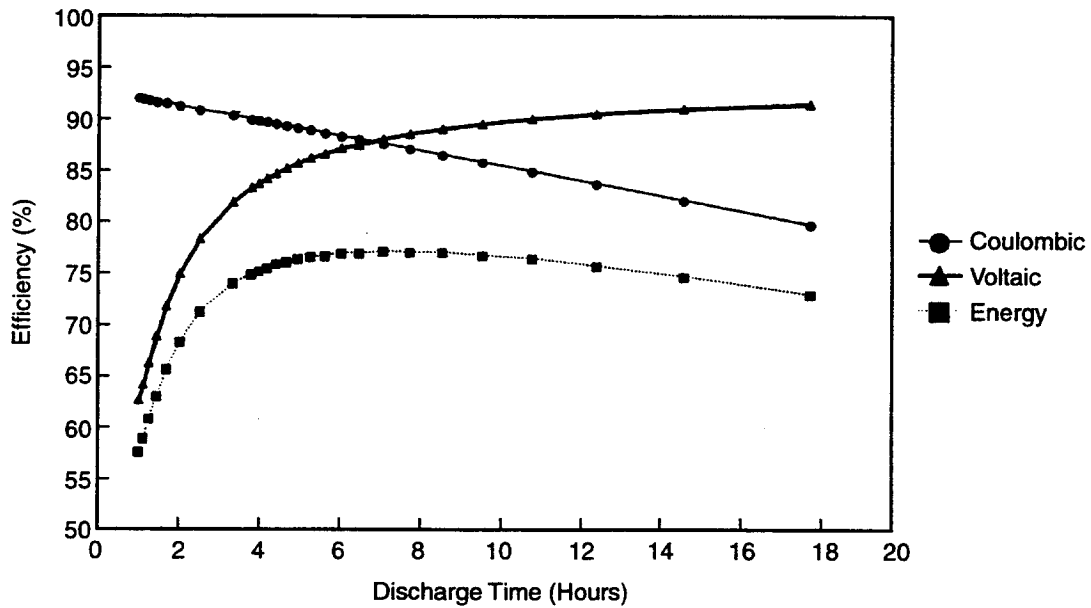


Figure 2-11. Effect of discharge time on efficiencies (standard 8-cell stack, no pumping losses).

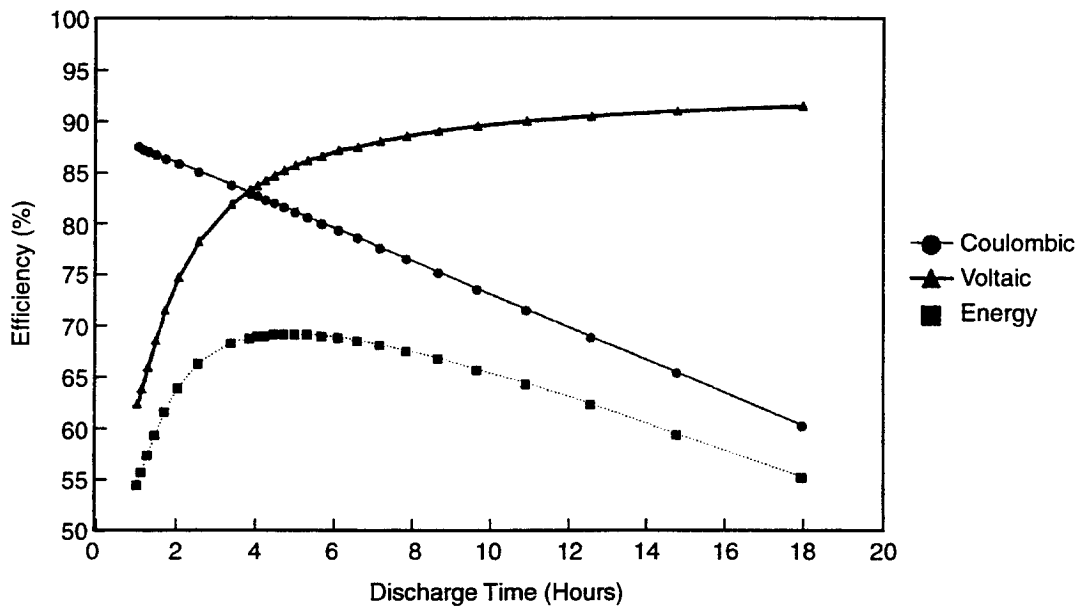


Figure 2-12. Effect of discharge time on efficiencies (standard 8-cell stack with pumping losses).

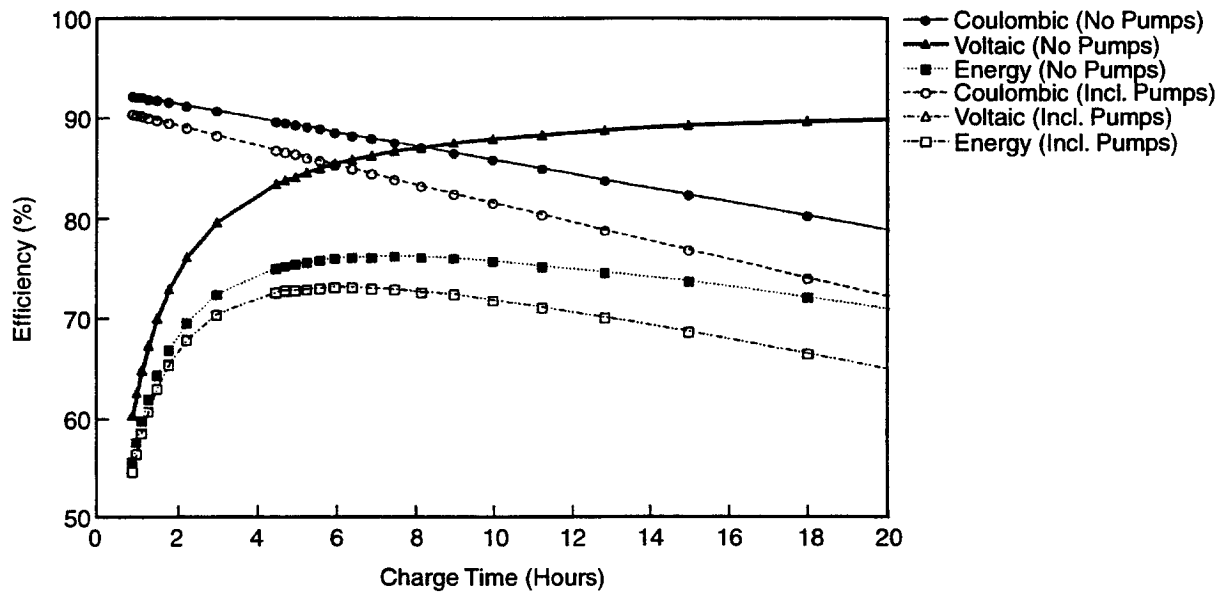


Figure 2-13. Effect of charge time on efficiencies (zinc/bromine 8-cell stack with and without pumping losses).

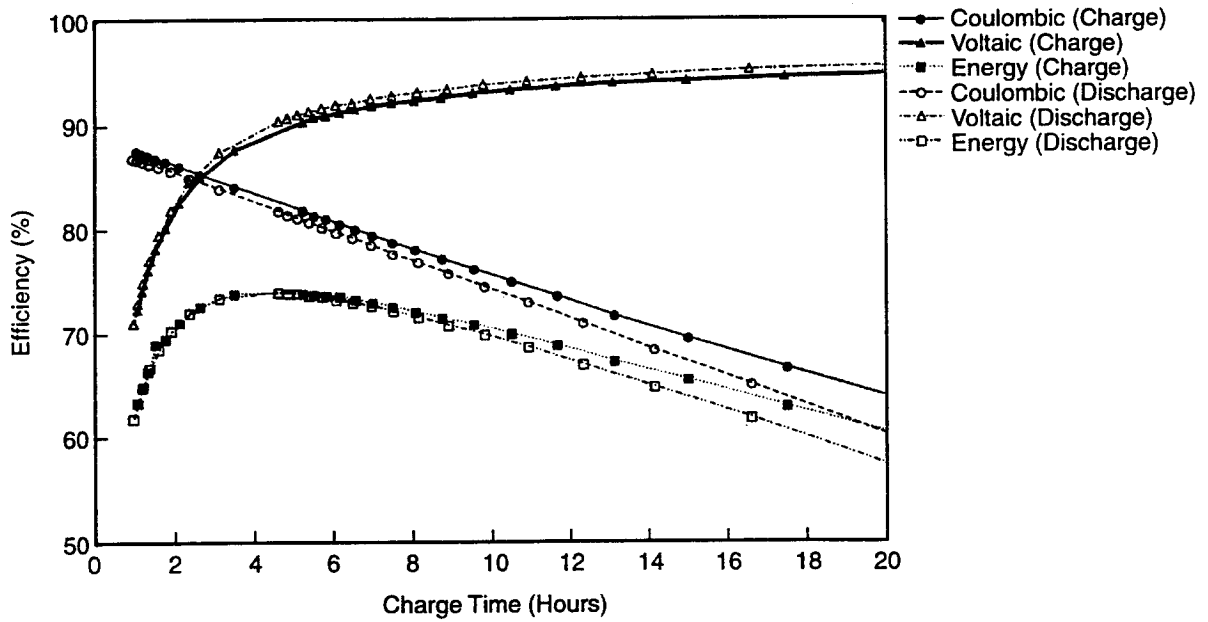


Figure 2-15. Effect of charge and discharge times on efficiencies (80-cell system with pumping losses).

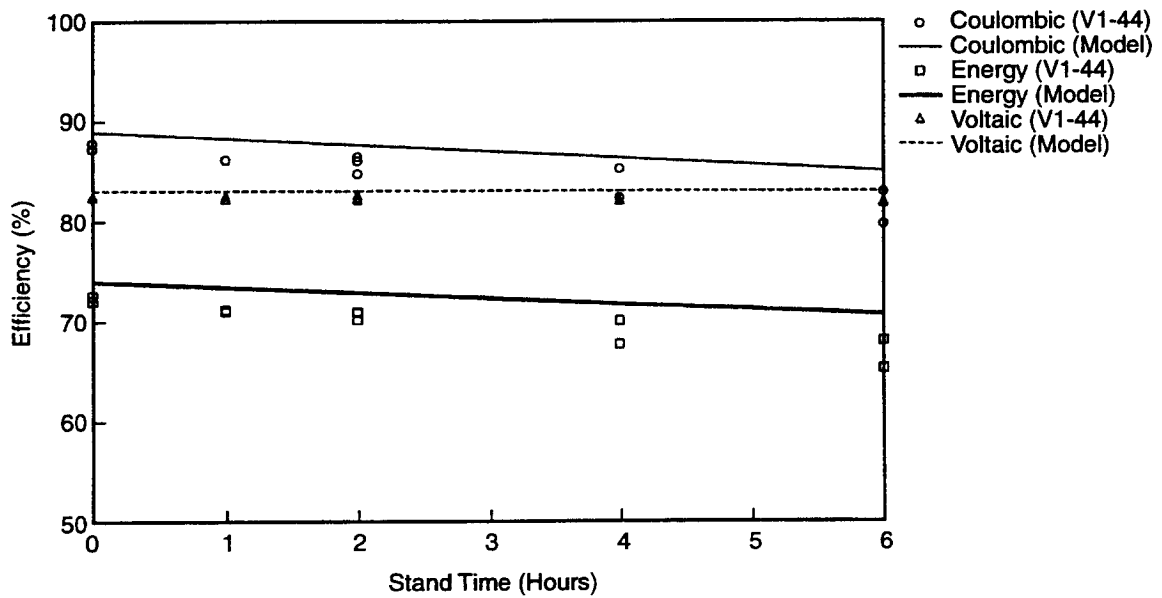


Figure 2-16. Stand time study for Battery V1-44 compared to model predictions.

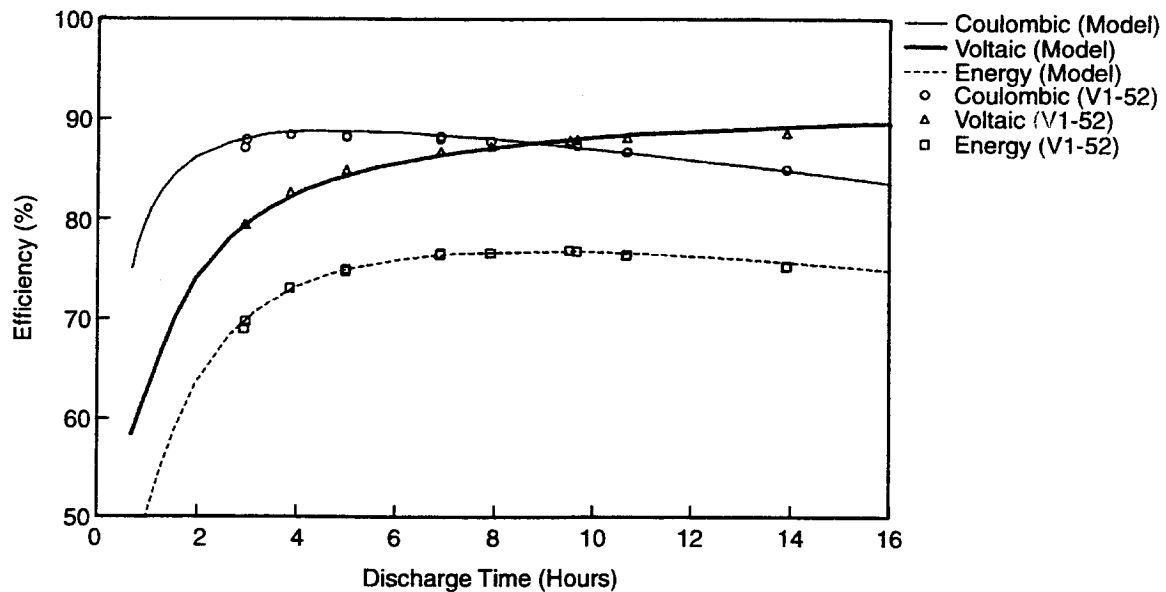


Figure 2-14. Effect of discharge time on efficiencies – Battery V1-52 versus model.

current density. An empirical relationship between residual losses and discharge current density was added to the computer model to adjust for this fact. This enables a very good correlation between the model and actual results as seen in Figure 2-14.

Similar analyses were performed for an 80-cell (2300-cm² electrode) battery system (a projected deliverable). The effects of discharge and charge times can be seen in Figure 2-15 for an 80-cell battery system including pumping losses. Results are similar to the results observed for an 8-cell battery system. The best energy efficiencies could be obtained with about a 5-hour charge and a 5-hour discharge. By increasing or decreasing these times, the performance will decline because of either coulombic or voltaic effects.

Stand Testing

A new attribute of the computer model is the capability to calculate efficiencies when stand times (open circuit) are added to the charge/discharge cycles. This enables the model to simulate real load-leveling duty cycles. The computer program estimates losses because of bromine transport and shunt currents during open circuits of a given duration. Results of stand times from 0 to 6 hours are compared to the stand test results for Battery V1-44 in Figure 2-16. The model gives slightly higher efficiencies than the battery, but the battery was not running at peak performance dur-

ing the tests. Even though the model results do not exactly match the battery results, the general downward trend in energy and coulombic efficiencies are similar.

New Battery Design Optimization

Optimization studies were run for an 80-cell battery system (a projected deliverable) with and without considering shunt-current losses. Iterations over the channel dimensions, manifold diameter, and anolyte and catholyte gaps were run to determine the dimensions that would give the optimum battery performance. Initial estimates for the cell parameters came from doubling the sizes used in the present battery design. Results of the optimization can be seen in Table 2-4 for cases with and without shunt-current losses.

The results in Table 2-4 indicate that optimum energy efficiencies could be obtained with anolyte and catholyte gaps of 0.015 inches. These results are based only on pumping, shunt current, and resistivity trade-offs. Considerations other than efficiency could include air bubble formation and uneven zinc plating (caused by poor flow) at higher loadings if the anolyte gaps are made too small. Consequently, the best configuration would be a 0.015-inch catholyte gap with a 0.020-inch anolyte gap.

Table 2-4. Cell Stack Optimization

	Including Shunt-current Losses		No Shunt-current Losses	
	Original	Optimized	Original	Optimized
Manifold diameter (in.)	0.625	1.0	0.625	1.0
Channel length (in.)	25.0	25.0	25.0	12.0
Channel width (in.)	0.24	0.50	0.24	0.40
Anolyte gap (in.)	0.032	0.015	0.032	0.015
Catholyte gap (in.)	0.032	0.015	0.032	0.015
Coulombic %	81.1	82.2	83.0	86.7
Voltaic %	87.4	90.1	87.3	90.0
Energy %	70.9	74.1	72.5	78.1

Safety Study

An investigation into the various safety factors of the zinc/bromine battery has been initiated. The perception that bromine is dangerous presents a possible roadblock to the acceptance of zinc/bromine batteries. In fact, exposure to bromine is the only serious hazard of the battery other than electrical shock, a hazard shared by all technologies. With the exception of the eyes, bodily contact with the battery electrolyte is fairly benign.

There is little or no pure bromine in the battery. The bromine that is present is found as either Br_3^- ion in the aqueous portion of the electrolyte, or as quaternary complexes in the "red oily phase" of the electrolyte. Both forms of bromine have greatly reduced activity and volatility compared to elemental bromine. Testing has focused on the quaternary complex because the second-phase contains nearly all of the bromine that might escape from the battery.

To properly understand the bromine hazard such as it would occur in a load-leveling facility, it is necessary to make reasonable estimations of the following:

1. The concentration at which bromine becomes dangerous.
2. The rate of evaporation expected from an electrolyte spill.
3. The degree of dispersal and dilution of the bromine vapors.

The lowest concentration at which an animal or human has been known to die is called the lethal con-

centration low. For bromine, the concentration is 180 ppm, which was lethal to rabbits after seven hours of exposure. However, the odor of bromine gas becomes distressing when inhaled at concentrations at about 15 ppm.² If possible, a person will take action to get away and will avoid being exposed to injurious levels of bromine.

The bromine evaporation rate has not as yet been measured, but the vapor pressure can be found. The measurements of the total pressure over the polybromide complex in 100% state-of-charge load-leveling electrolyte (Figure 2-17) show how the pressure increases with temperature. The values measured were slightly higher than those reported for MEPBr complex in the "Factory Mutual Study."³ However, when the composition of the vapor was tested by titration, it was found to be only about 50% bromine. The remainder was probably mostly water of hydration in the complex.

The safety enhancement of bromine complex formation is apparent from Figure 2-17. The pressure of bromine (uncomplexed) is so high that it boils (that

² J.C. Bailar-Ed. 1973. *Comprehensive Inorganic Chemistry*, p. 1231. Pergamon Press Limited, Elmsford, New York.

³ R. Zalosh, and S. Bajpai. 1981. "Comparative Hazard Investigation for a Zinc-Bromine Load-Leveling Battery," Final Technical Report for EPRI Project RP1198-4, Vol. 26, p. 2.

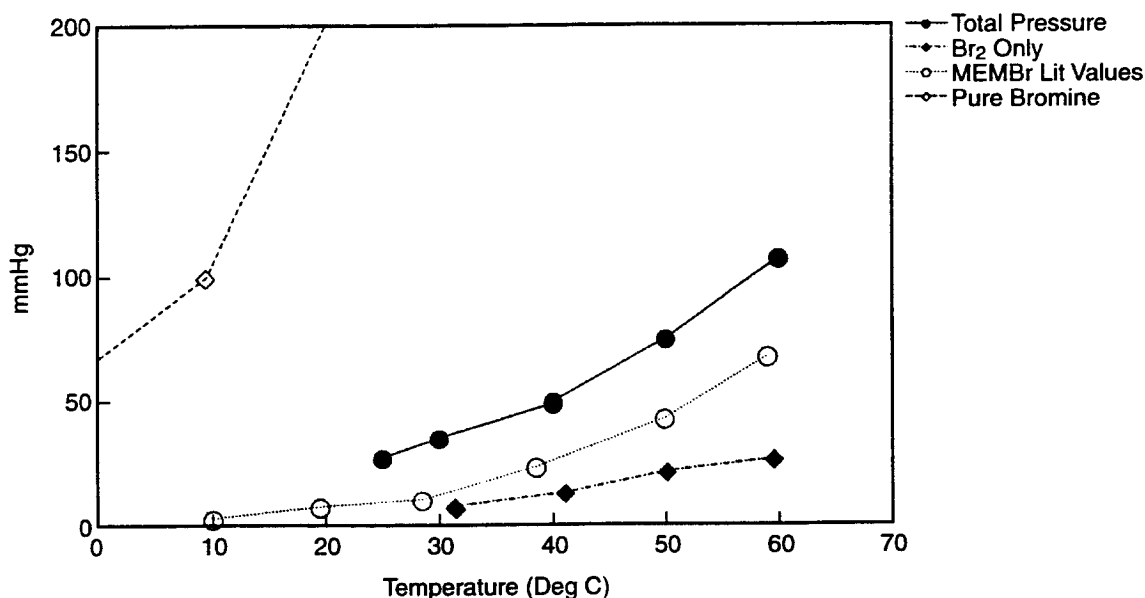


Figure 2-17. Vapor pressures over MEPBr complex.

is, the vapor pressure equals atmospheric pressure) at about 60°C. But when complexed, the bromine pressure is only 10% of atmospheric pressure at 60°C.

Electrolyte Recycling Program

The electrolyte in the zinc/bromine battery has shown no evidence of deterioration over time. Only contamination of the used electrolyte would prevent immediate electrolyte reuse. Some possible sources of contamination might be internal corrosion from the stack or station, and sloppy handling and storage in "dirty" containers. In earlier studies on the electric vehicle program, some impurities, especially electroplatable transition metals, were found to be readily removable.

A preliminary plan was proposed for the handling of recycled electrolytes. An outline of the processes is shown in Figure 2-18. The major steps are: analysis for purity and composition, treatment to reduce transition metals, and filtration. If the recycling process can be carefully controlled so that the electrolyte is removed from old batteries without introducing new contaminants, it should be possible to return it to service easily with only a cursory check of the purity and composition. The more electrolyte that can be recycled without having to repurify it, the less expensive the process will be.

Undoubtedly, some material will be nonrecyclable for various reasons. There are two possible ways to recover valuable electrolyte materials from this waste. First, zinc could be separated by electrodeposition, and then reacted with the bromine that would evolve at the counter electrode to reconstitute pure ZnBr₂. Second, the zinc could be precipitated by adjusting the pH to alkaline. The remaining NaBr solution would be purified of metals by ion-exchange. The NaBr could be converted to HBr and NaOH by a "water splitting membrane" process, and the HBr reacted with the ZnO to regain the ZnBr₂. A good way has not yet been found to purify the quaternary agents. Possibly, separation could be effected from a contaminated aqueous solution by use of bromine to form a second-phase.

The two main analytical tools needed for electrolyte recovery will be an inductively coupled plasma (ICP) analyzer for determining ppm levels of metals, and an ion chromatograph for doing composition/concentration analysis of the electrolyte. An x-ray fluorescence machine might be substituted for the ICP. At present, only a few analyses are done per week. In a recycling facility, the number might go up to several dozen per day. This means the analytical procedures will need to be automated and have a low cost per sample. Ion chromatography and ion capillary electrophoresis methods should be able to provide accurate, rapid analyses of the electrolyte composition, using equipment that is relatively inexpensive.

Electrolyte In

- Source
 - Known
 - Segregate
 - o Electric Vehicle
 - o Load Leveling
 - Neutralize Bromine
 - Analyze Purity, Evaluate & Mix
 - Pure
 - Impure w/metals
 - Zinc treatment
 - Carbon filter
 - Impure w/solids
 - Particle filtration
 - Analyze Concentration
 - OK
 - Concentrated
 - Dilute with water
 - Dilute
 - Make up with concentrate
 - Return to service
 - Not recyclable
 - Source Unknown
 - Neutralize bromine
 - Analyze Components
 - Assign electrolyte type
 - Analyze Purity, Evaluate and Mix
 - Pure
 - Impure/metals
 - Zinc treat → Carbon filter
 - Impure/solids
 - Particle filter
 - Analyze Concentration
 - OK
 - Concentrated
 - Dilute with water
 - Dilute
 - Make up with concentrate
 - Return to service
 - Not Recyclable

Figure 2-18. Electrolyte recycling processes.

Ion capillary electrophoresis equipment is claimed to be capable of resolving ppm concentrations of most ions. If this is true, it might be preferred over the ICP. Also, recent advances in the electrochemical technique, anodic stripping voltammetry, allow it to resolve ppm levels of most transition metals (basically anything that can be plated out of aqueous solution). The major difficulty in this particular application is the high background of ZnBr₂.

The critical test will be to determine whether the different procedures are capable of analyzing real electrolyte. Future plans will include sending samples of the clean and dirty electrolyte to each of the equipment suppliers. From the quality of their results and the cost of their apparatus, decisions about which process to use can be made. Table 2-5 below is a short summary of the methods of analysis and applications.

Table 2-5. Type of Analysis

	Impurity	Com- position
Inductively coupled plasma	✓✓	
Anodic stripping voltammetry	✓	
Ion chromatography	✓	✓✓
Ion capillary electrophoresis	✓	✓✓

✓ = might give satisfactory results.
✓✓ = likely or known to give satisfactory results.

Adhesive Bonding

It is possible that the battery assembly process could be accelerated if the stacks were put together using adhesive bonding instead of vibration welding. There has been much recent progress in new structural adhesives that can bond to polyethylene and are chemically inert. Three adhesives were selected for testing from a number of commercially available alternatives.

Samples of the glass-fiber-reinforced frame plastic were cut to two-inch coupons and glued with either wide beads (using the whole frame width, about

0.5 inches) and narrow adhesive beads (the size of the weld bead, 0.08 inches). Some samples were exposed to bromine vapor for five days; others were exposed to sulfuric acid for five days. They were then tensile-tested to failure.

A list of the samples and test results is shown in Table 2-6. The surface preparation was critically important to the adherence of the joint, as can be seen in the results of the tensile tests. All samples were cleaned with acetone, but the plastic was still too slippery unless it was specially prepared. Samples that were treated with chromic acid and physically roughened with sandpaper were noticeably stronger.

TYPE II adhesive did not appear to be as strong as TYPE I, and TYPE II overheated when it was mixed so that much of the adhesive in the mixing pot was lost. Because it was more difficult to work with and showed no advantage over the other adhesives, it was not used in the chemical exposure tests.

Samples of TYPE I and TYPE III adhesives were tested for adherence and resistance to two chemicals: bromine vapor and sulfuric acid. The adherence tests are listed in Table 2-6. The data in Table 2-6 are given in pounds per inch of glue bead and so are readily comparable to vibration-weld data. Both adhesives had softened after five days in bromine vapor, but TYPE I was still holding tightly, while TYPE III had nearly fallen off. In five days of exposure to sulfuric acid, TYPE I was almost unaffected, while TYPE III showed some surface crazing.

The results of the adhesive testing are shown in Figure 2-19. The narrow glue bead was not as strong as a vibration weld of the same size. However, a wide glue bead was quite strong. In fact, two of the samples broke before the glue to plastic bond did. The narrow glue bead samples showed the effect of exposure to bromine. It could be seen that the bead softened in the bromine, then became brittle when the bromine evaporated. The sulfuric acid had little or no apparent effect on the TYPE I samples, but did affect the TYPE III samples. Wide glue bead samples did not seem to be affected, but in time, they probably would be.

Table 2-6. Adhesive Bonding Tests on Polyethylene

Sample	Bead	Adhesive Type	Failure Load Pounds/inch	Chemical Exposure	Surface Preparation
9A	Narrow*	TYPE I	75.2		Chromic acid
10A	Narrow*	TYPE I	55.6		Chromic acid
11A	Wide	TYPE I	142.5		Chromic acid, roughened
12A	Wide	TYPE I	124.8		Chromic acid, roughened
5A	Narrow*	TYPE II	20.9		
6A	Narrow*	TYPE II	25.2		
7A	Wide	TYPE II	50.9		Roughened
8A	Wide	TYPE II	60.1		Roughened
13A	Narrow*	TYPE I	56.3	H ₂ SO ₄	Chromic acid
14A	Narrow*	TYPE I	52.1	H ₂ SO ₄	Chromic acid
15A	Narrow*	TYPE I	56.1	Bromine	Chromic acid
16A	Narrow*	TYPE I	12.2	Bromine	Chromic acid
20A	Narrow*	TYPE III	72.3		Chromic acid
19A	Narrow*	TYPE III	36.0	Bromine	Chromic acid
17A	Wide	TYPE III	Tab**		Chromic acid, roughened
18A	Wide	TYPE III	Tab**	H ₂ SO ₄	Chromic acid, roughened

* All narrow adhesive beads were milled, but not further roughened.

** Tab means the base material failed before the bond.

In summary, one adhesive (TYPE I) was identified that could be used to bond plastic parts in sulfuric acid service, but would not work as well in zinc/bromine electrolyte. Another adhesive (TYPE III) provided a strong bond, but should not be used where it would be exposed to any battery electrolyte. Despite the lower chemical resistance, the TYPE III adhesive wetted the plastic surfaces well

and gave excellent adherence values. In fact, the tabs on the wide bead samples failed before bonds. This adhesive could be used for station assembly work. If used for stack assembly, both adhesives should be applied in a wider bead than the vibration weld. If that is done, the bond can be as strong as a vibration weld, and certainly would be suitable for service in applications with no chemical exposure.

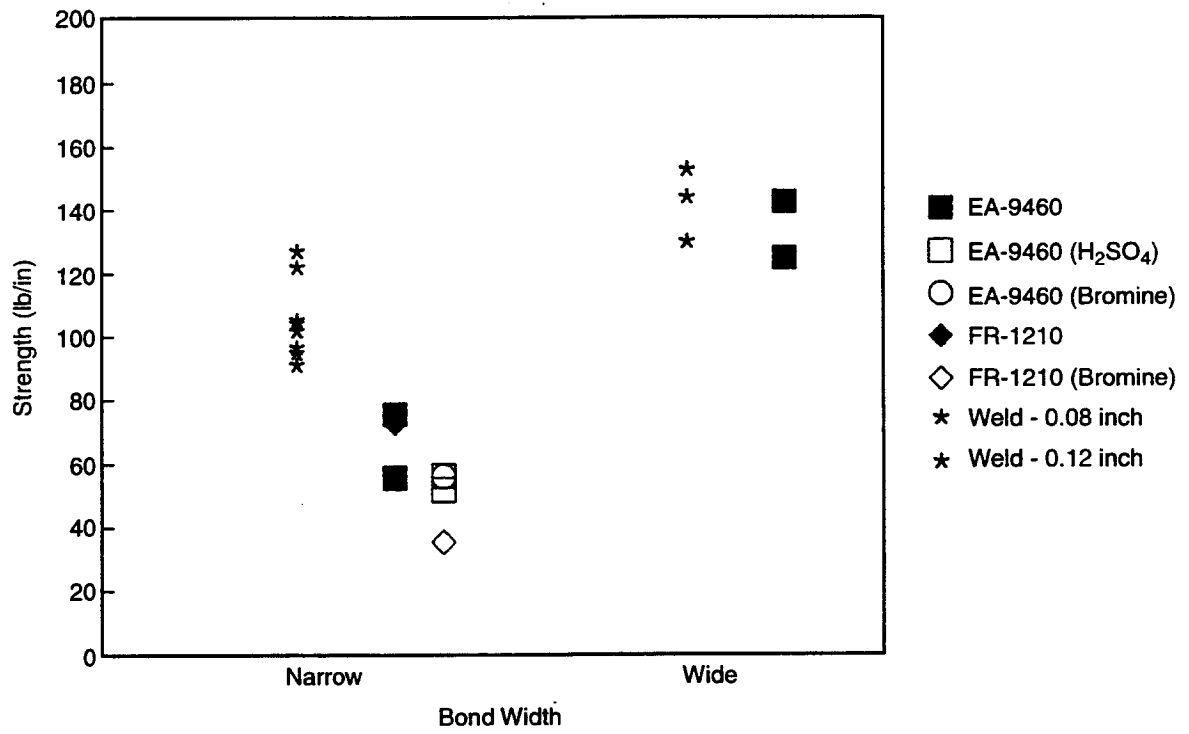


Figure 2-19. Adhesive bonding strength.

Intentionally Left Blank

3. Other Laboratory Test Results

Miniature Cell Tests

Miniature single-cell batteries have been fabricated with half the active electrode area of a standard V-design battery. They were developed to investigate the effects of factors such as operating conditions (for example, charge-current density, zinc loading), electrolyte composition, and battery materials. The miniature cells not only use smaller amounts of materials, but can be opened to inspect the quality of the zinc. The initial work on the miniature cells, or "minicells," has been to establish baseline performance levels for the cells, to investigate the effects of plating current density on zinc dendrite formation, and to test samples of chemically treated separator. Two miniature cells were used in these laboratory tests.

Current Density Studies

To test the effect of current density on zinc plating, cycles were run at charge-current densities ranging from 20 mA/cm² to 50 mA/cm², with the zinc loading held constant at 90 mAh/cm². Recall that the baseline cycle is run at a charge-current density of 20 mA/cm² with the total zinc loading at 90 mAh/cm². No fewer than three complete charge/discharge cycles were run in each test, after which the cell was opened and inspected at 100% state of charge to observe the zinc plating. Before each set of cycles, a baseline cycle was run to compare battery performance with previously run cycles.

Figure 3-1 shows the effect of charge-current density on efficiencies for minicell No. 2. The main effect of increasing current is a decrease in voltaic efficiency caused by ohmic current/internal-resistance (IR) losses associated with the higher current density. The coulombic efficiency appears to increase slightly as current density is raised. This is presumed to be caused by the reduced time available for bromine transport at higher current densities.

The size of the decrease in performance may be exaggerated in Figure 3-1 because of an overall reduction in performance of the minicell during baseline cycles (see Figure 3-2). The general downward trend

in voltaic efficiency as the number of cycles increases is most likely caused by corrosion of the copper screen in the terminal electrodes. The minicell electrodes were prepared with only one layer of carbon plastic on the active side of the electrode; standard terminal electrodes were made thicker. This was done to lower the cell resistance so it would be comparable to that of a single cell in a full-size battery. This trade-off raises the voltaic efficiency at the expense of long life. In earlier minicells made with the standard terminal electrode construction, the voltaic efficiency was low because the carbon plastic available at the time was too resistive. Future electrodes will be made with thicker carbon plastic. The newer carbon plastic is less resistive, so the voltaic performance should be adequate.

Tear-downs of the cell at 100% state of charge did not show any significant differences between cycles run at different charge-current densities. The zinc plated at 40 mA/cm² looked essentially the same as the zinc plated at 20 mA/cm². Zinc, which was slightly dendritic in appearance, was seen near the outside edges of the electrode when the cell was inspected at 100% state of charge after a 50 mA/cm² (1.8-hour) charge. Charge-current densities were increased until poor zinc plating was observed at 60 mA/cm². In the next set of tests to be carried out in Phase 2 of the program, plating additives will be introduced to the system to determine what concentrations will be needed to obtain smooth zinc plating.

Separator Testing

Minicells are also being used to test various separators. Samples of Asahi separator were coated with a sulfonated polyester resin at SNL. The coated material was compared to uncoated Asahi separator by cycling at standard conditions. Results are shown in Table 3-1.

The coated separator gave a coulombic efficiency increase of 2% by decreasing the bromine transport. The voltaic efficiency decreased by about 1% because of the slightly higher resistivity of the coated separator. The net increase in energy efficiency was about 1%.

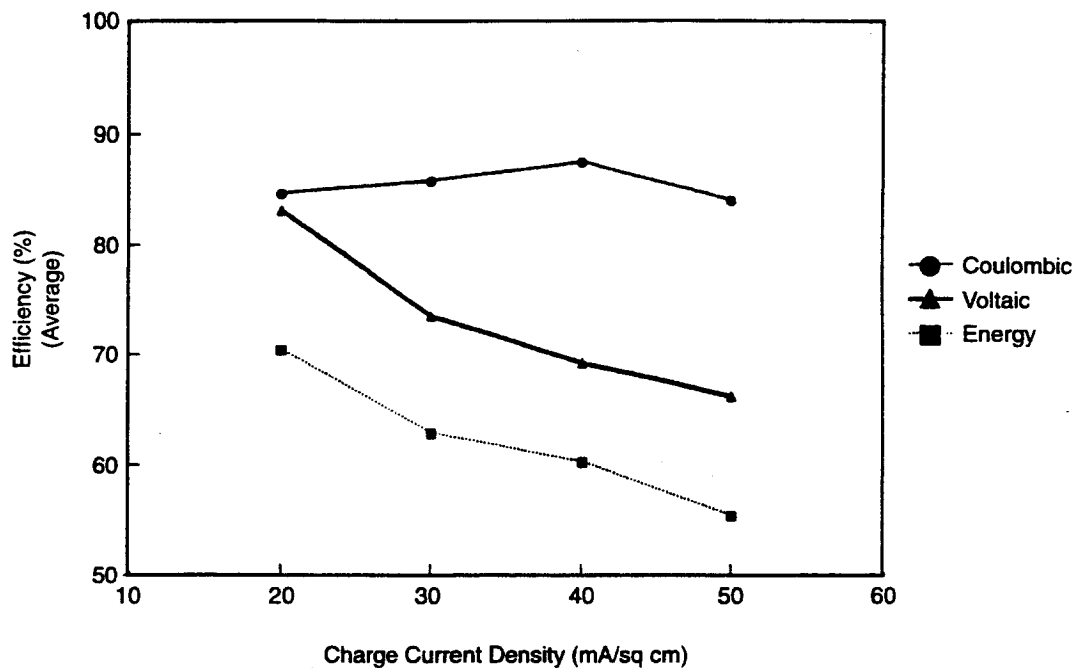


Figure 3-1. Effect of charge-current density on efficiencies (Minicell #2).

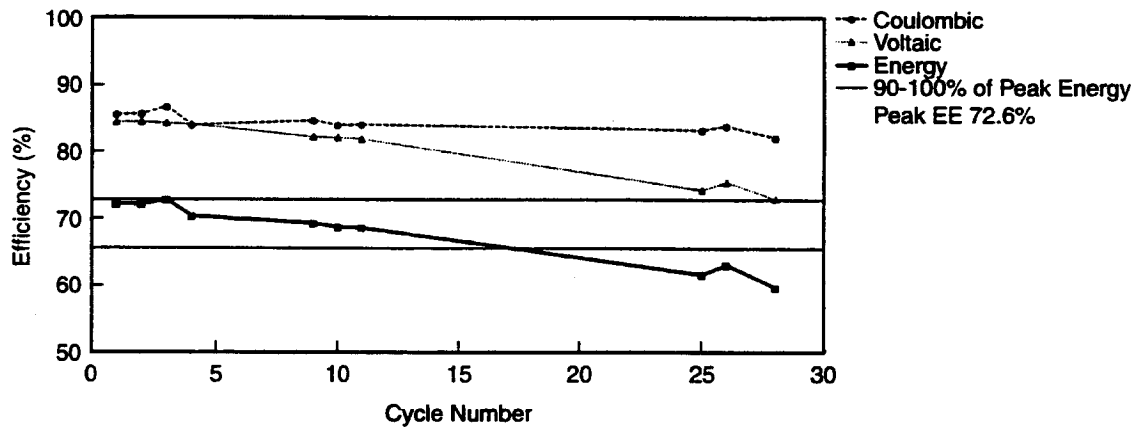


Figure 3-2. Baseline cycle efficiencies (Minicell #2).

Table 3-1. Separator Comparison

	Coulombic Efficiency (%)	Voltaic Efficiency (%)	Energy Efficiency (%)	Transport Inefficiency (%)	Residual Inefficiency (%)
Standard	86.4	80.2	69.3	11.4	2.2
Chemically Coated	88.4	79.3	70.1	8.9	2.4

Zinc Plating

Testing Methods

Various tests were performed using 6-cm² flow-by test cells to better understand factors that affect zinc-plating morphology. Screening studies were performed to determine how such factors as charge-current density, zinc loading, electrolyte flow rates, and plating additives affect plating in various electrolytes. The primary electrolyte used was unsupported ZnBr₂ (zinc bromide) solution with a 50/50 mixture of methylethylmorpholinium (MEM) bromide and methylethylpyrrolidinium (MEP) bromide quaternary ammonium complexing agents. In some tests, potassium chloride (KCl) was added to enhance the conductivity. The zinc plating was found to get rougher with increasing charge-current density and zinc loading. Electron spectroscopy for chemical analysis (ESCA) surface studies have also been used to help identify the causes of rougher zinc plating, which is normally observed in the presence of KCl-supported electrolytes. These studies indicated that the rougher plating in KCl-supported electrolytes could be caused by a greater propensity toward zinc oxide surface growths.

Zinc-plating morphology was examined both qualitatively and quantitatively. Photographs of zinc plating samples were taken for visual comparisons under the various testing conditions. Dendrite heights were measured from the tip of the dendrite to the base of the zinc plate using an optical microscope. Five dendrites of about average height (eliminating very large and small dendrites and edge effects) were measured to obtain an average dendrite height. Using calipers, the thickness was measured from the back side of the plate to the tip of the largest peak.

Zinc Loading and Current Density

Dendrite heights were plotted versus zinc loading at a constant current density of 18 mA/cm² and versus current density at a constant zinc loading of 90 mAh/cm². Figure 3-3 gives the results for unsupported electrolyte with and without additives. Figure 3-4 gives the results for unsupported and KCl-supported electrolytes. Figure 3-3 shows that dendrite height increases with zinc loading, which could be expected. It also shows that plating additives can be effective in reducing dendrite formation, even at very high zinc loadings of 180 mAh/cm². Figure 3-4 illustrates that dendrite height increases with increas-

ing current density, and that 3 M KCl-supported electrolyte gives rougher plating than an unsupported electrolyte at a given current density.

Some reports in the scientific literature have indicated that zinc-plating morphology in acid media may become smoother if plating current densities are increased to 100 mA/cm² or greater.^{1,2} To verify the information in these reports, studies were conducted at very high flow rates compared to the standard laminar flow conditions in JCBGI's plating studies. Experiments of up to 65 times the standard flow rate and up to 200 mA/cm² were completed to examine these factors. In every case, zinc plating appeared rougher at higher current densities for both unsupported and KCl-supported electrolytes. The data in Figure 3-5 show that the measured dendrite height decreases as the flow rate becomes very large. Also, at each flow rate, the lower current density gives a smoother surface for both unsupported and supported electrolytes, with the supported electrolytes being rougher than the unsupported electrolytes in each case. It has been concluded that high charge-current densities should be avoided to minimize dendritic growth at both high and low flow rates.

Even though the dendrites appear to be smaller at higher flow rates, there is still no evidence that a smoother surface should be observed as the current density becomes very large. The size of the largest zinc dendrites can be compared at various flow rates by observing zinc thickness measurements given in Figure 3-6. This figure indicates that even though the size of the dendrites on the surface of the plate may be smaller at high flow rates, some very large dendrites still do exist at high current densities, even at high flow rates.

ESCA Surface Studies

In other experiments, ESCA surface spectroscopy studies of zinc-plating samples were used to determine if zinc oxide formation on the electrodes influences the zinc-plating morphology.

¹ J.L. Faltemier. 1983. "The Effect of Hydrodynamic Flow on the Morphology of Electrodeposited Zinc," Ph.D. Thesis, University of California, Berkeley, California.

² C. Tobias, and J.L. Faltemier. December 1983. Proceedings of the EPRI/LBL Workshop on the Electrochemistry of Zinc/Halogen Batteries.

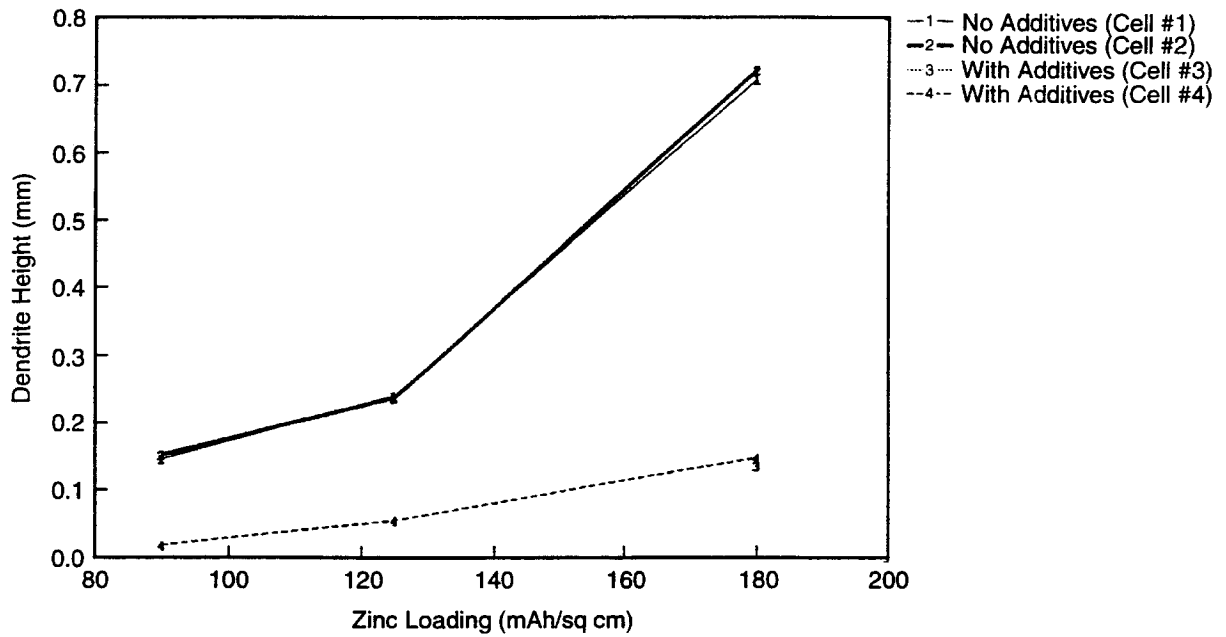


Figure 3-3. Effect of zinc loading on dendrite height – unsupported load-leveling electrolyte (constant current density of 18 mAh/cm²).

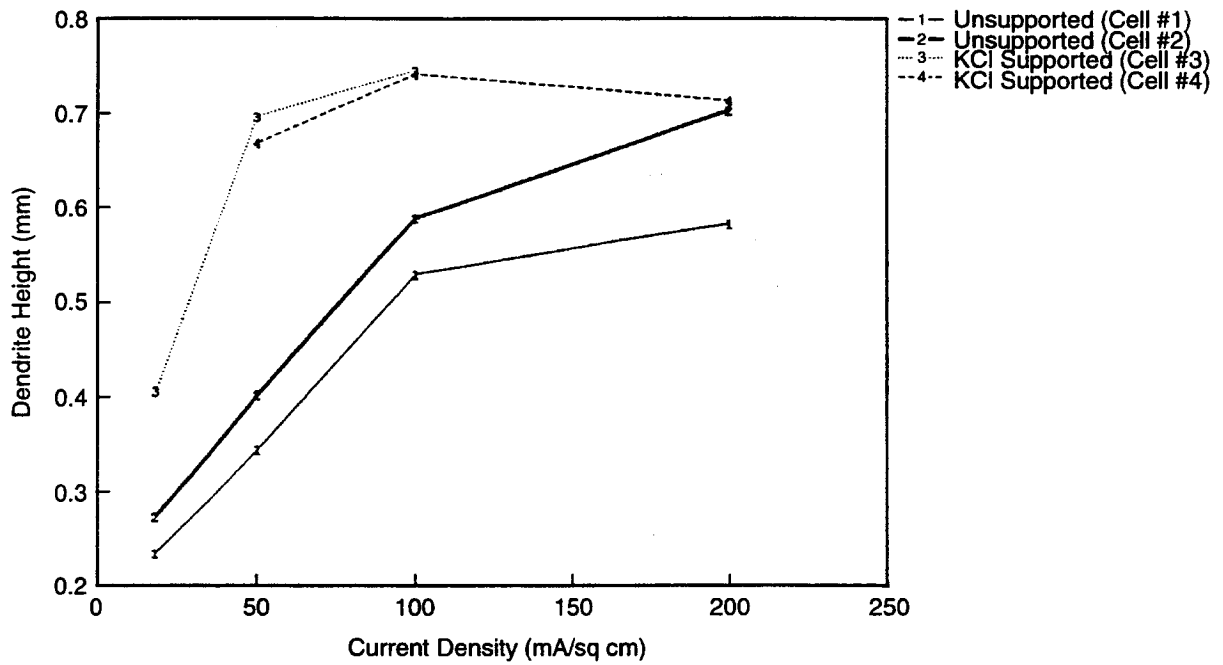


Figure 3-4. Effect of current density on dendrite height (constant zinc loading of 90 mAh/cm²).

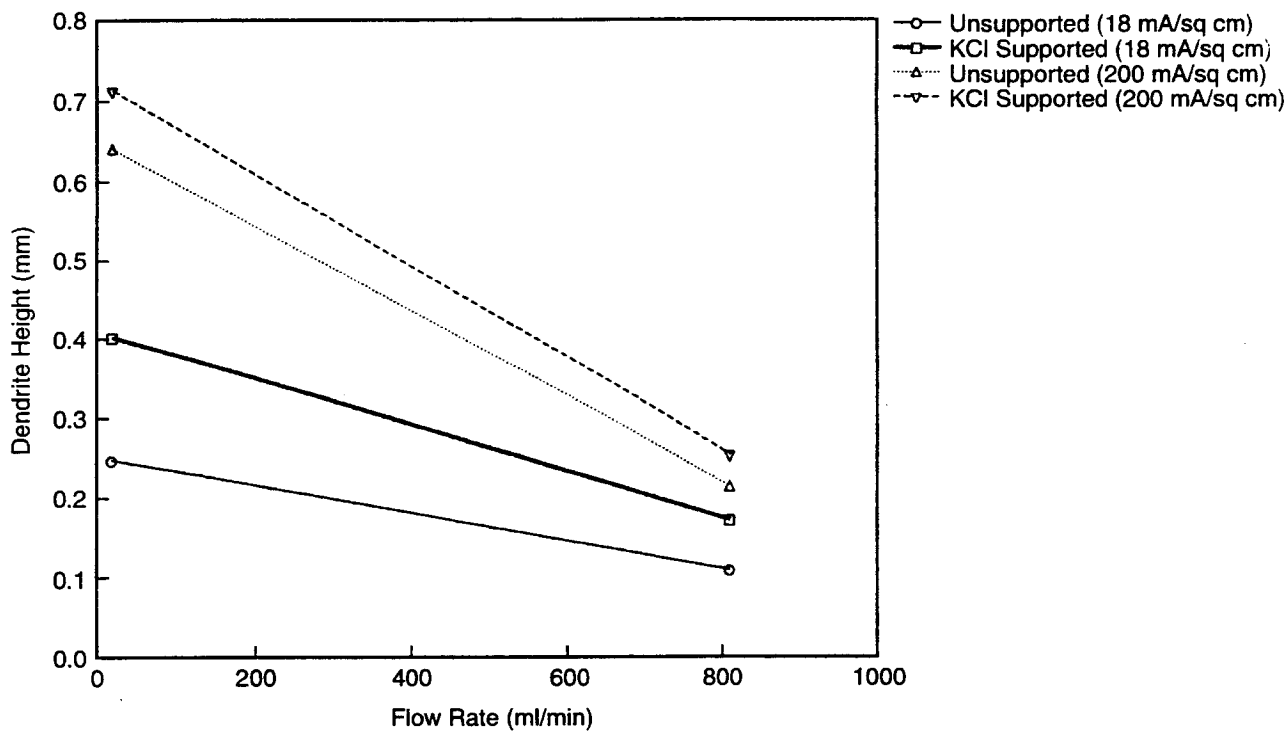


Figure 3-5. Effect of flow rate on dendrite height.

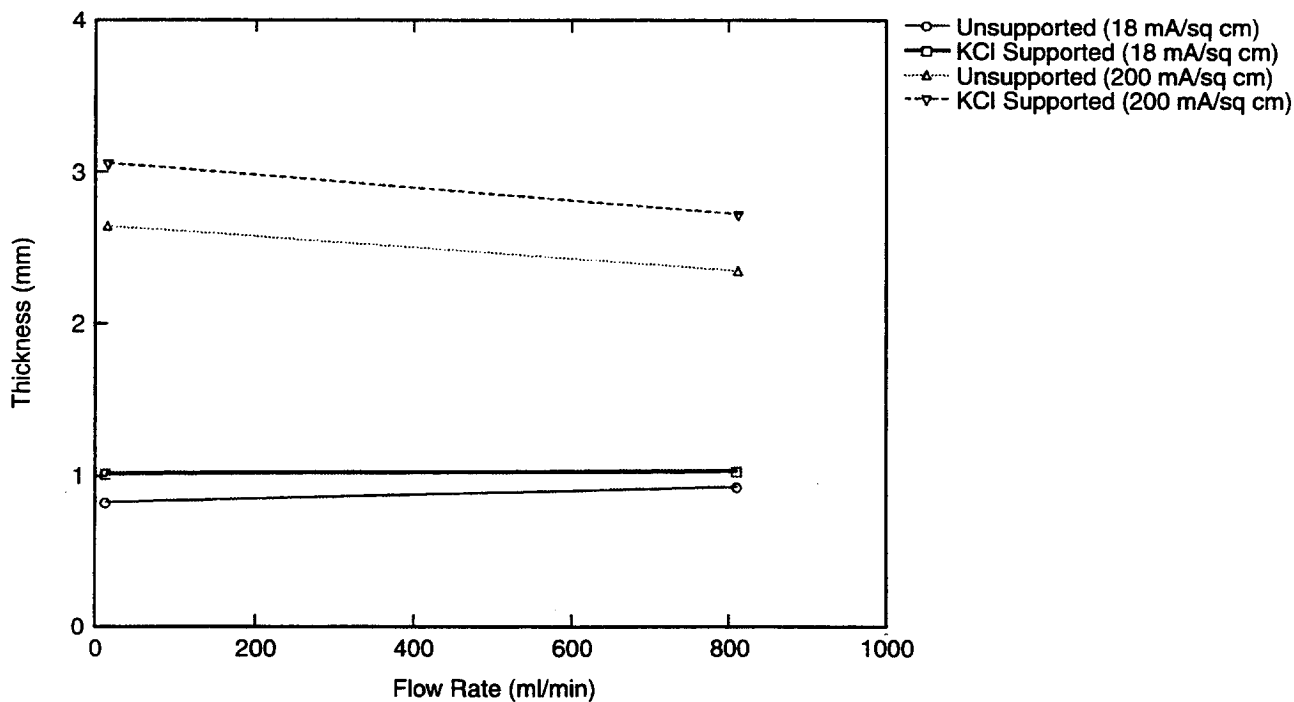


Figure 3-6. Effect of flow rate on zinc thickness.

Zinc oxide surface layers were consistently about two times thicker on zinc that had been plated from KCl-supported electrolytes than on zinc from unsupported electrolytes. There were no observed differences in trace-adsorbed impurities on the surfaces of these two types of zinc plating samples. Argon gas purging of the cell both before and during zinc-plating did not decrease the thickness of the zinc-oxide surface layers. This indicates that the oxide is not forming because of dissolved oxygen in the electrolyte. Instead, the zinc oxide layer is likely forming when zinc metal reacts with water and forms hydrogen gas as a co-product. This reaction appears to be fairly rapid and self-limiting, because the oxide layer thicknesses were essentially the same for samples exposed to the electrolyte for 30 or 240 minutes at open circuit following plating.

Argon-ion sputtering inside the ESCA instrument was used to determine the approximate oxide layer thicknesses. Therefore, it was possible that differences in surface roughnesses between the two types of plating samples, supported or unsupported electrolytes, could have artificially influenced their relative oxide thickness determinations. Consequently, follow-up experiments were performed to measure zinc oxide thicknesses on the smooth back faces of the zinc-plating samples which had been peeled away from the carbon-plastic electrode backbones. The electrodes were then immersed at open circuit for 30 minutes in the different electrolytes. As before, the samples were then transferred to the ESCA instrument under an argon atmosphere. The smooth back faces of these electrodes had oxide surface layers that were 3 to 10 times thinner than that of the front electrode surfaces which were exposed to electrolyte throughout plating. However, just as before, the electrodes that were exposed to KCl-supported electrolytes, exhibited oxide surface layers that were approximately two times thicker than those of electrodes plated in unsupported electrolytes.

The ESCA experiments indicated that a greater propensity for zinc oxide formation could be the cause for the rougher zinc plating, which is observed in KCl-supported electrolytes. The zinc plating additive package could be improving zinc plating by reducing zinc-oxide surface thicknesses by at least 20%. Zinc-oxide surface growths could cause rougher zinc plating by creating surface heterogeneities, which act as dendrite precursor sites. Experiments will be conducted in unsupported load-leveling electrolytes to determine if zinc oxide growths cause rougher zinc plating onto unstripped, partially discharged zinc layers.

In summary, it has been shown that the KCl-supported electrolyte consistently gives rougher plating than the unsupported electrolyte, and that an increased tendency toward zinc oxide formation is a possible cause for this increased roughness. Incorporation of JCBGI's proprietary zinc-plating additives has yielded very smooth plating at loading levels as high as 180 mAh/cm².

Bromine Electrode

Background

To date, most of the full-size test batteries at JCBGI have been constructed using bromine electrodes that contain conventional PV-2 type cathode activation layers. These electrodes have generally shown good performance, at least up to the presently achieved 300 charge/discharge battery cycles. However, a variety of beaker-scale experiments have been done to further ensure the optimal fabrication, performance and long-term cycle life of bromine electrode activation layers.

A new electrochemical surface area measurement technique was developed. The results of these tests, coupled with ESCA carbon-surface analyses, indicated that declines in bromine electrode performance with increasing accelerated cycle life in beaker-scale tests may be attributed to changes in carbon surface chemistry, as opposed to simple physical loss of electrode surface areas. ESCA surface studies of various types of cathode layer carbons identified how carbon surface chemistries can be optimized to improve the long-term cycle life performance of bromine electrodes.

Based on work done before this contract, JCBGI decided that carbonaceous-type electrode surfaces, such as the PV-2 porous carbon layer, are the materials of choice at this time. In addition, methods to fabricate the porous carbon layers are being studied. These include ways to apply the carbon, because the original method is more suited to laboratory preparation rather than to mass fabrication. Results will be reported as part of Phase 2.

Electrochemical Surface Area

During accelerated life-cycle testing, the electrochemical performance of bromine test electrodes declines with increasing cycle life. A surface area measurement technique was required to determine

whether this declining electrode performance was caused by a simple physical loss of electrode surface area (for example, spalling off of surface carbon). BET surface area measurements have not proven sensitive and reproducible enough to measure the bromine electrode surface areas, especially if the areas are less than about 1000 cm² actual area per cm² geometric area.

A cyclic voltammetric technique was developed to more accurately determine the electroactive surface areas of bromine test electrodes. The technique measures double layer capacitance, which is directly proportional to the electroactive surface area of the electrodes. Using this technique, it was determined that neither PV-2, nor CP-4 carbon-paper-type cathode layers lose their electroactive surface area during accelerated life-cycle testing. Therefore, the declines in electrode performance were attributable to something other than physical losses in electrode surface areas. As described later, ESCA studies indicated that changes in carbon surface chemistry were the likely cause of declines in electrode performances during accelerated life-cycle testing.

Optimization of Surface Chemistry

ESCA surface spectroscopy has been used to monitor the changes in carbon surface chemistry during the life-cycle testing of various types of cathode layer carbons. In essentially all cases, the carbons lose graphitic character and gain in surface oxygen content during accelerated charge/discharge cycling. Based on these findings, it is proposed that the best long-life bromine electrode carbons should have an optimum combination of high graphite content, low oxygen content, and high surface area. Pure graphite powder did not perform well in a cathode layer owing to the naturally low surface area of very highly graphitic carbon. Thus, there are some restrictions as to just how highly graphitic the carbons can be. However, partial graphitization and removal of surface oxygen from a poor-cycle-life carbon converted it into one of the best cycle-life carbon cathode layers.

Bromine electrodes containing powder PV-2 or heat-pressed CP-4 carbon paper cathode layers were analyzed by ESCA surface spectroscopy as a function of cycle number during accelerated life-cycle testing. The ESCA analyses were run on a V.G. Scientific Model VG ESCALAB instrument which was located at the University of Wisconsin at Milwaukee. The ESCA oxygen 1s peak at 531 eV was used to measure changes in surface oxygen contents of the carbons,

while the carbon energy loss region of 305 to 315 eV was used to monitor changes in the graphitic character of the carbons. The peak intensity at 314 eV is a measure of the amount of delocalized electron character, that is, graphitic content of the carbons, while the peak intensity at 305 eV is a measure of the amorphous content of the carbons. The ratio of these peak intensities was taken to be a semi-quantitative measure of the ratio of graphitic to amorphous content of the various cathode layer carbons.

The bromine 3d peak at 70 eV was also monitored to measure changes in the amount of strongly bound bromine. The bromine content of all electrodes remained at about 2 atom percent independent of the cycle number. This bromine was undoubtedly chemically bound to the carbons, because weakly adsorbed bromine would have been removed during the successive aqueous and acetone rinses of the electrodes, which were followed by vacuum treatments longer than 24 hours before their introduction into the ESCA instrument. The bromine content of the carbons did not correlate with their life-cycle performance. However, as described below, an increasing oxygen content and decreasing graphitic character of the carbons appeared to correlate with the increasing polarization of the cycling electrodes.

The 4-cm² bromine test electrodes were subjected to accelerated life-cycle testing, which consisted of a total of 7000 10-min. charge/10-min. discharge cycles at a current density of 100 mA/cm². The tests were conducted over a 3-month period at room temperature in a simulated constant 35% state of charge catholyte electrolyte. The relatively high current density used in this cycling has been shown to accelerate the degradation of the cathode activation layers.

The correlation between battery cycle life and these accelerated cycles is such that the 7000 accelerated cycles are believed to approximately correspond to about 2000 battery cycles. However, this correlation is quite tenuous because it is primarily based on the testing of a limited number of battery electrodes, which had less than 200 cycles. Thus, right now the accelerated life-cycle testing is used mainly as a comparative screening tool for various types of cathode activation layers. IR-free polarization curves were taken every 1000 to 2000 cycles to periodically monitor electrode performance as a function of cycle life. Following the polarization tests, washed bromine electrode samples were submitted for ESCA analyses.

Figure 3-7 shows the polarization versus accelerated cycle-life data for both the PV-2 powder and the CP-4 carbon paper cathode layers. As described in the previous section, the observed increases in electrode polarizations with increasing cycle life were not caused by physical losses in electrode surface areas. Figures 3-8 through 3-11 show plots of amorphous/graphitic (A/G) carbon ratios and surface oxygen contents versus electrode polarizations for PV-2 and CP-4 carbon layers. There is some scatter in the data, but increasing oxygen content and increasing amorphous/graphitic carbon ratios appeared to correlate with the increasing electrode polarizations that were observed with increasing cycle numbers.

With the exception of the PV-2 surface oxygen data, multiple regression statistical analyses showed that the aforementioned correlations were statistically significant with greater than 90% confidence. The correlation between PV-2 oxygen and polarization was significant at only a 76% confidence level. Still, analyses of cathode-layer carbon types other than CP-4 and PV-2 have always shown an increase in oxygen content as well as decreasing graphite content after 7000 cycles. Therefore, JCBGI is fairly confident in making the statement that increasing the oxy-

gen content and decreasing the graphite content of cathode-layer carbons affect the increase of electrode polarization during increasing cycle numbers.

The correlation between carbon surface chemistry and cycle life has been further confirmed by treating a carbon to increase its graphite content and decreasing its oxygen content to improve the carbon's cycle-life performance. A high surface area wood-based carbon was found to give good initial polarization performance, but this polarization increased to unfavorably high levels after only a modest 1000 accelerated cycles. The carbon supplier was asked to treat this given batch of carbon to increase its graphitic content and lower its oxygen content. This treatment increased the ratio of graphitic/amorphous carbon from 1.22 to 1.58, while decreasing the surface oxygen content from 8 to 4 atom percent. As seen in the polarization plots of Figure 3-12, the high-graphite-content, low-oxygen-content carbon showed much better cycle-life performance than the original carbon, which had low graphite and high oxygen content. Also note that this improved wood-based carbon was performing significantly better after 5900 cycles than PV-2 after 5000 cycles.

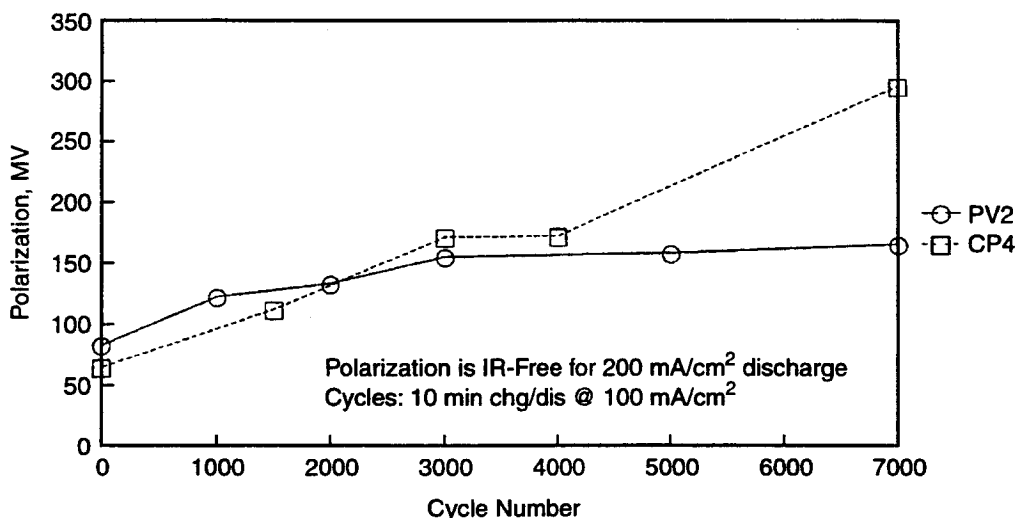


Figure 3-7. Polarization versus cycle life for PV-2 vs. CP-4 carbon paper electrodes (data is average of >2 electrodes per run).

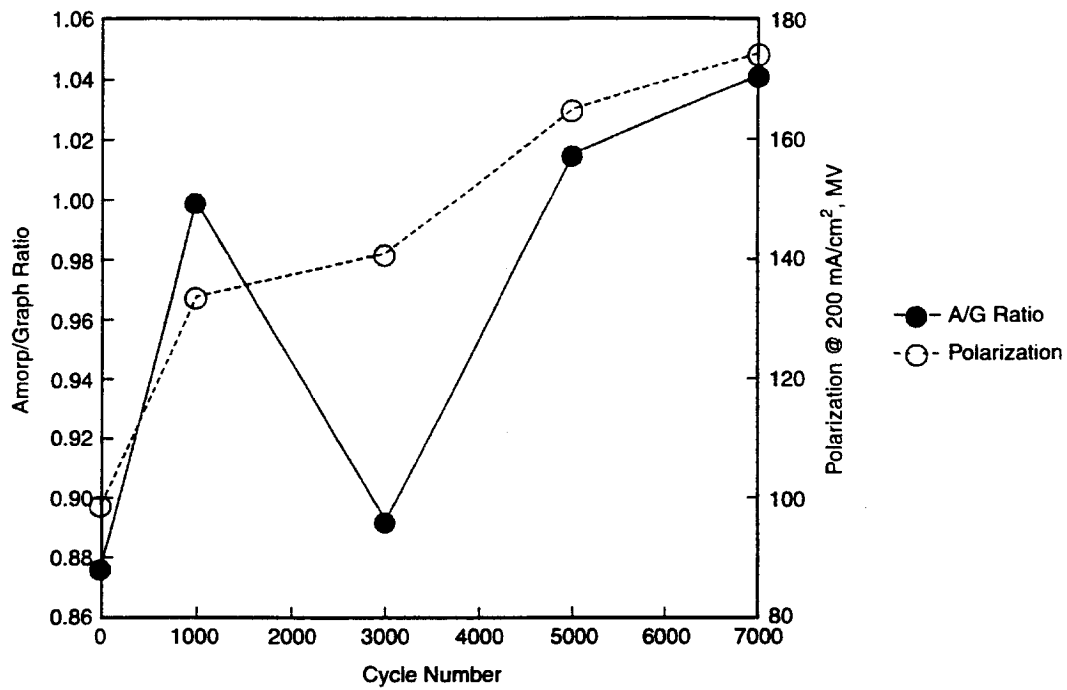


Figure 3-8. ESCA-monitored changes in amorphous/graphitic carbon ratios for PV-2 carbon.

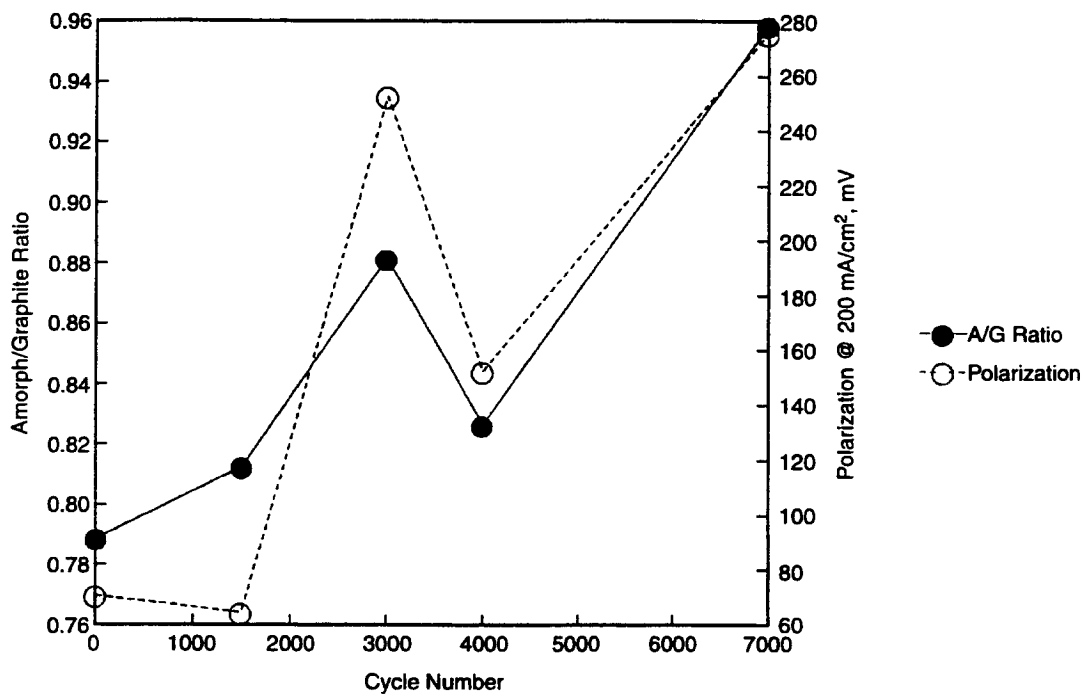


Figure 3-9. ESCA-monitored changes in amorphous/graphitic carbon ratios for CP-4 paper carbon.

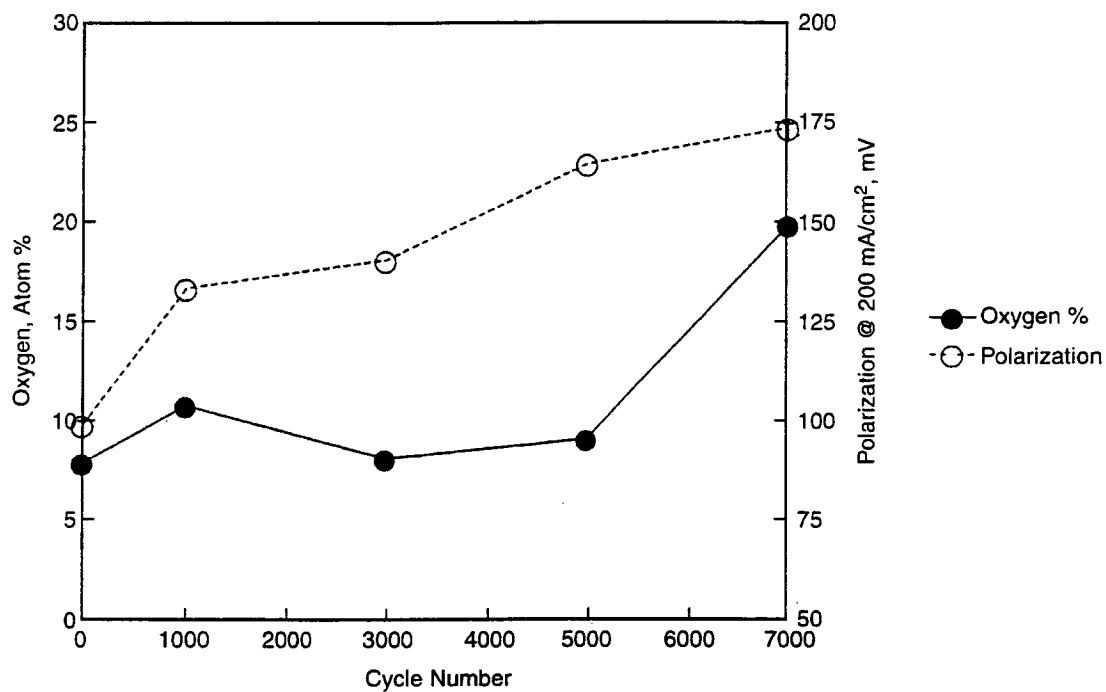


Figure 3-10. ESCA-monitored changes in amorphous/graphitic carbon ratios for PV-2 carbon.

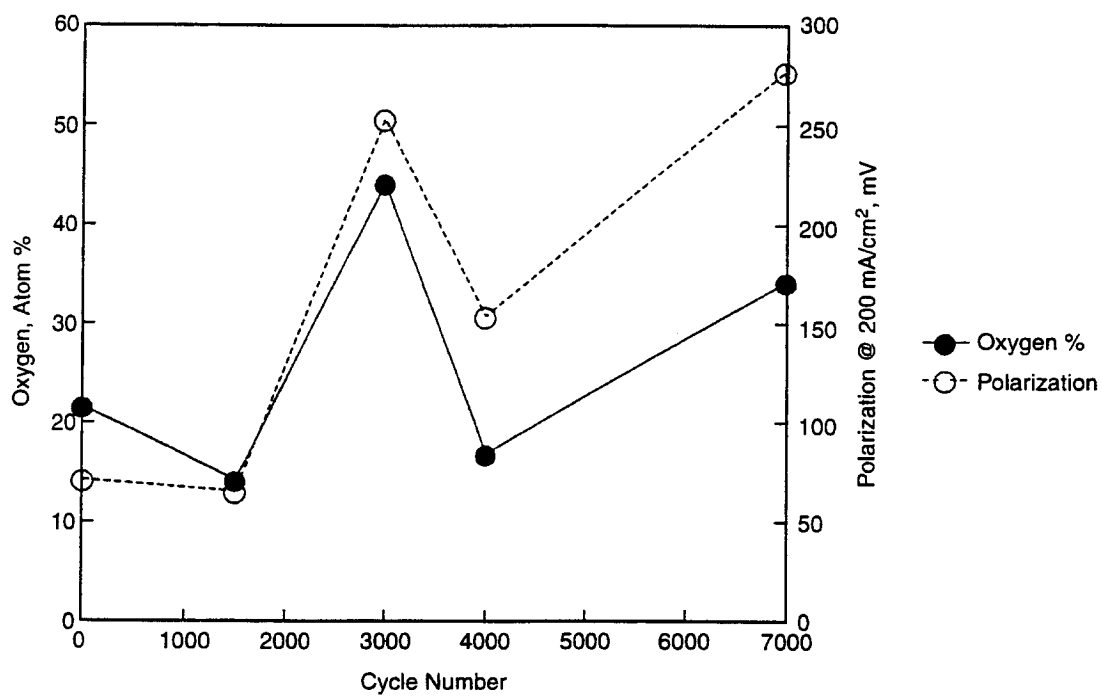


Figure 3-11. ESCA-monitored changes in amorphous/graphitic carbon ratios for CP-4 carbon.

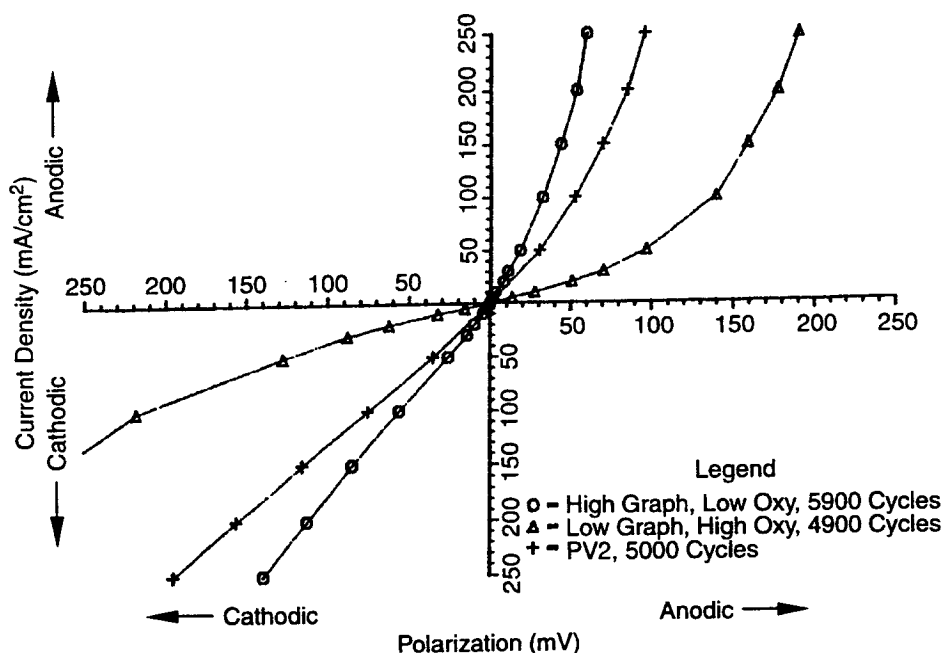


Figure 3-12. Polarization plots, high graphite, low oxygen.

Electrolyte Composition

Consideration of some of the basic properties of electrolyte leads to the conclusion that higher energy efficiencies may be attainable by using a more dilute electrolyte composition. Naturally, this entails some sacrifice in energy density, but this may be warranted for load-leveling batteries where energy density is not a primary consideration.

Previous zinc plating studies have shown that the unsupported electrolyte tends to produce better quality zinc plating, with higher coulombic efficiencies, than supported electrolyte. Also, lower concentrations of zinc bromide tend to give better zinc plating. These observations may be at least partially explained by the fact that less complexation occurs in an electrolyte with lower concentrations of halide ion (either Br^- or Cl^-). Complexation can make zinc ions in solution less available for the zinc ion reduction reaction ($\text{Zn}^{++} + 2e^- \rightarrow \text{Zn}^0$).

In addition to improved coulombic efficiency, the use of a more dilute electrolyte would, under certain conditions, be expected to produce improved voltaic performance. Figure 3-13 shows the resistivity of zinc bromide solutions, methylethylprolidinium bromide (MEPBr) solutions, and mixed $\text{ZnBr}_2/\text{MEPBr}$ solutions as a function of concentration. Note that for the

mixed solutions, the resistivity decreases as the ZnBr_2 concentration is decreased, until it reaches a minimum at 1 molar. The data suggest that the voltaic efficiency of batteries currently being investigated may improve slightly by substituting the present concentration of 2.25 M ZnBr_2 with a more dilute composition (such as 1.8 M). It must be pointed out that a sufficient volume of electrolyte must be available so that at the end of charge the zinc bromide concentration does not become significantly lower than the concentration at which the resistivity is lowest (1 M in this case). If the concentration becomes too dilute, the resistivity becomes high again.

Studies with more dilute electrolyte are under way on Battery V1-59. At Cycle 17, the standard load-leveling electrolyte composition of 2.25 M ZnBr_2 , 0.55 M ZnCl_2 , 0.8 M MEPBr was replaced by a similar composition electrolyte with 1.83 M ZnBr_2 . Figure 3-14 shows the improvement obtained using the more dilute electrolyte. Contrary to expectations, most of the improvement was in coulombic efficiency, with a slight decrease in voltaic efficiency. The energy efficiency underwent a slight, but statistically significant improvement of 0.7%.

These studies will continue at lower zinc loadings in Phase 2 of the contract. The lower loadings will result in a smaller ZnBr_2 concentration change throughout the cycle.

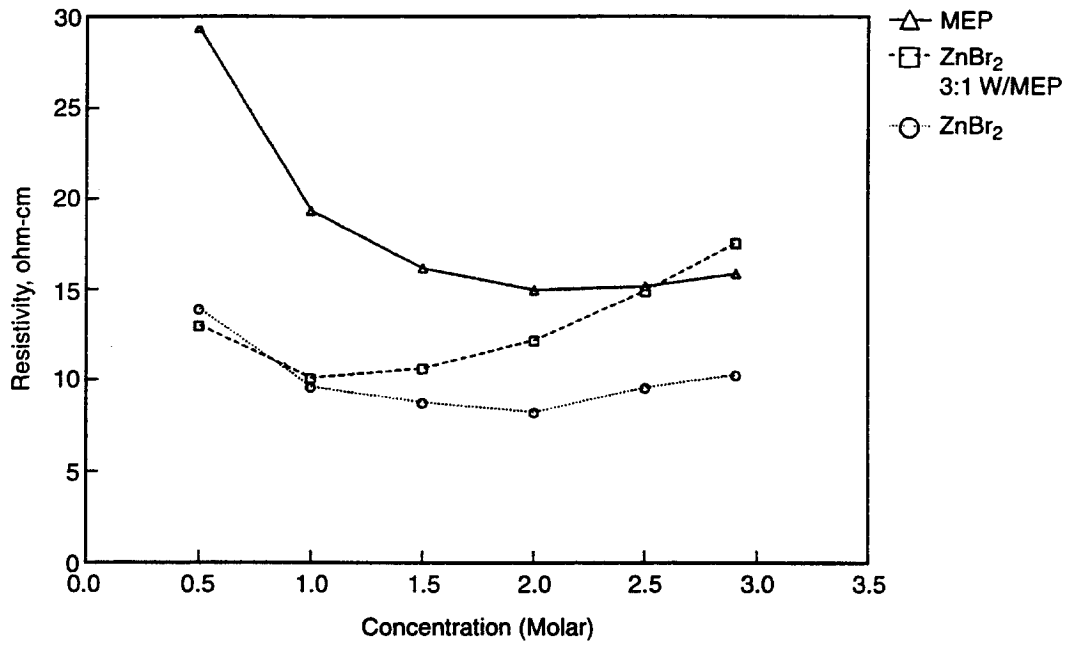


Figure 3-13. Resistivity of ZnBr₂, MEPBr, and mixes versus concentration.

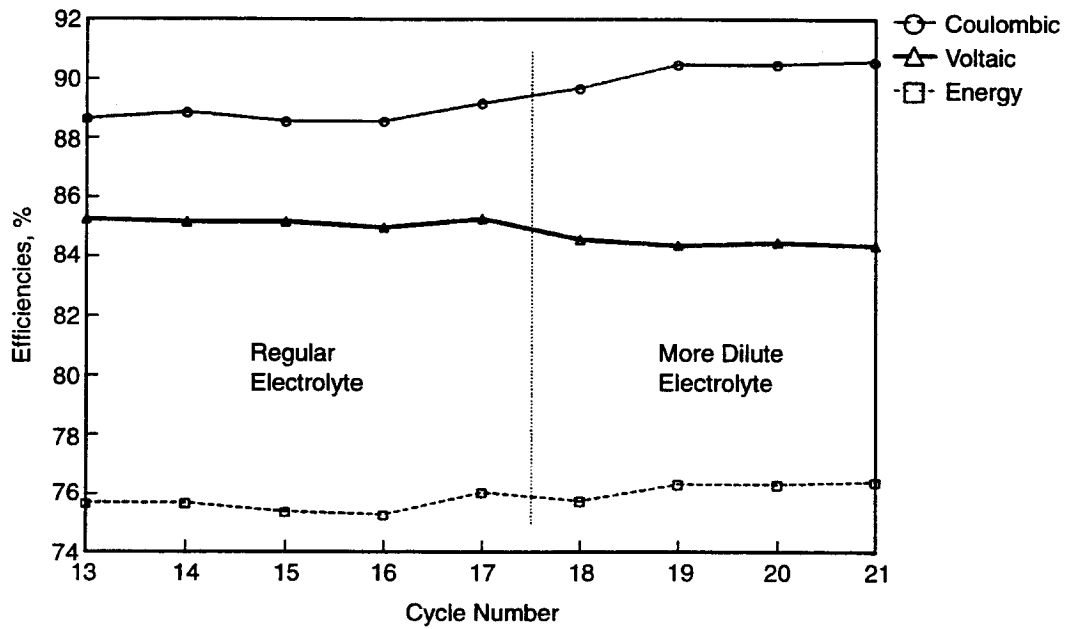


Figure 3-14. Electrolyte dilution test for Battery V1-59.

4. Battery/Station Design

Cooling

The heat that is generated by a battery can be estimated from the efficiency of operation. Every kilowatt-hour not utilized in discharge is converted to heat. Recently tested batteries have shown typical energy efficiencies of 70 to 75%. For every 1 kWh of energy delivered in discharge, 1.43 to 1.33 kWh must be charged, and 0.43 to 0.33 kWh of heat will be released. Therefore, the starting point for determination of battery cooling requirements is to use a design value of about 40% of the battery energy capacity.

The JCBGI 8-cell battery station typically uses 36 inches of 1/4-inch-diameter titanium tubing for the heat exchanger. Cooling water flows through the tubing, and warm electrolyte is on the outside. The tubing is placed where it will contact the returning anolyte. The cooling water is supplied from the tap, at a temperature of about 13°C in the JCBGI labs. Because titanium tubing is costly, other materials should be considered for better cost-effectiveness. Plastic tubing has been used in a larger station.

Data from Battery VL-14 has been used as a starting point for designing the cooling system for the dual-stack 50-cell battery deliverable. VL-14 is a 50-cell (single stack) battery that has been satisfactorily kept at an operating temperature of 30°C by using 19 feet of 1/4-in. teflon tubing. The water inlet and outlet temperatures are typically 14°C and 17°C, respectively; the flow rate is about 0.75 gallon/min., and the water line pressure about 40 psi. The energy capacity of Battery VL-14 is about 7.5 kWh; therefore a cool-

ing capacity of about 3 kWh would be needed. The cooling data given above correspond to roughly 5 kWh, which is fairly good agreement.

Because the dual-stack deliverable battery will have a capacity of about 15 kWh, the cooling capacity of the next deliverable station should be twice that of Battery VL-14.

Pump/Motor Procurement

The centrifugal electrolyte pumps in recent use have been made of Ryton (polyphenylene sulfide) and have proven to be only marginally adequate for this application. Ryton is brittle, and it is very slowly attacked by bromine. Polypropylene pump heads identical to the Ryton pump heads have been used with limited success. However, a problem exists when they are used near the cutoff point, where the flow is throttled to a very low flow rate. The pump used for the 8-cell station is somewhat oversized. When the pump is throttled to restrict its outflow, the forward thrust on the impeller becomes excessive. This forward thrust is designed into the pump to compensate for the rearward thrust seen during normal operation. The front bearing supports of these polypropylene pump heads do not hold up for an acceptable length of time under these conditions.

The dual 50-cell station for the SNL deliverable battery used centrifugal pumps with polypropylene bodies. They are powered by the standard AC motors.

Intentionally Left Blank

5. Laboratory Battery Cycling Results

Battery Cell Stacks

Production

A large number of 8-cell and larger cell stacks were produced in the effort to refine the assembly process and to collect operating data. Some of the more significant changes in the production process included a new injection mold for the flow frame that had a more uniform electrolyte flow pattern, changes in the vibration weld surfaces and process, modified tooling on the welding machines and a change to a different welding machine. All together, 24 8-cell stacks and 7 larger stacks were produced during Phase 1.

Cycle Life

The standard cycle used for gathering baseline data consists of three steps. First is a 4.5-hour charge to 105 Ah (90 mAh/cm²) at 23.3 A, followed by a discharge at the same current to a cutoff voltage of 1.0 V per cell. The third part of each baseline cycle is full strip to zero charge. This is done by shorting the cell through a resistor. The amp-hour information collected during the strip is used to determine the transport and residual inefficiencies, which are components of the coulombic efficiency. The transport inefficiency is the part of the coulombic inefficiency caused by chemical transport of bromine across the separator to the anode chamber, where it chemically reacts with the electroplated zinc. The residual inefficiency is the portion caused by zinc and bromine remaining in the battery when the cutoff voltage is reached.

Table 5-1 shows the number of stacks built during specified time periods during Phase 1 and includes a comment on their resulting performance. In the early builds, a number of failures of the cell-stack welds occurred. This stopped when the vibration welds were improved. Further improvements in the welder and process have nearly ended unexpected weld failure. When an occasional weld failure does occur, it can generally be traced to a documented poor weld. Batteries V1-42 and V1-43 were made with an experimental carbon plastic that was discovered to be porous although initially it appeared sufficiently dense. Battery V1-61 was made with special thin

flow frames for increased power, but the flow was not sufficiently uniform to cycle well. Although the successful builds started with Battery V1-53, some later builds were short lived as changes in the cell stack building process were incorporated and problems were found and solved.

Table 5-1. Summary of 8-Cell Stacks Built In Phase 1

Time Period	Stacks Built	Comment
8/90 – 9/90	3	Stacks split open while cycling
10/90	1	Stack shorted by dendrites
12/90	2	Water slurry process electrodes proved porous
1/91– 3/91	7	Internal and external weld failures
2/91		Tooling on welder modified
3/91		Modified flow-frames phased in
3/91 – 4/91	7	Four stacks exceed 250 cycles, three stacks experience weld failure
5/91		Welding process moved to new machine
6/91	1	Cycled successfully
7/91		Improved flow frame introduced
8/91 – 9/91	3	One stack failed at weld during abusive test

Efficiency

The cell stacks routinely achieved efficiency percentages in the mid-seventies following the changes in production that strengthened and otherwise improved the welds. The cell stacks are able to maintain the high efficiency values for long periods, as shown by the efficiency plots for Batteries V1-53, V1-54, V1-55, and V1-57 (SNL518) (Figures 5-1 through 5-4). In these plots, the energy efficiency is maintained well above the 10% loss level for several hundred cycles. When batteries are taken off test, it is generally because of decreasing efficiency. At this time, work is under way to more closely identify the general causes of performance decline.

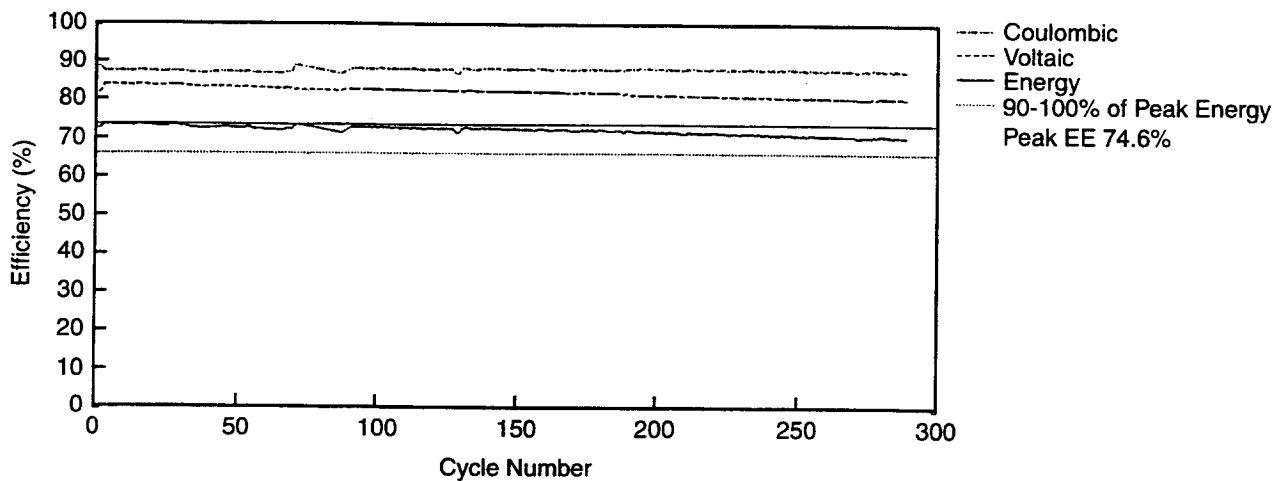


Figure 5-1. Stack V1-53 baseline cycle efficiencies.

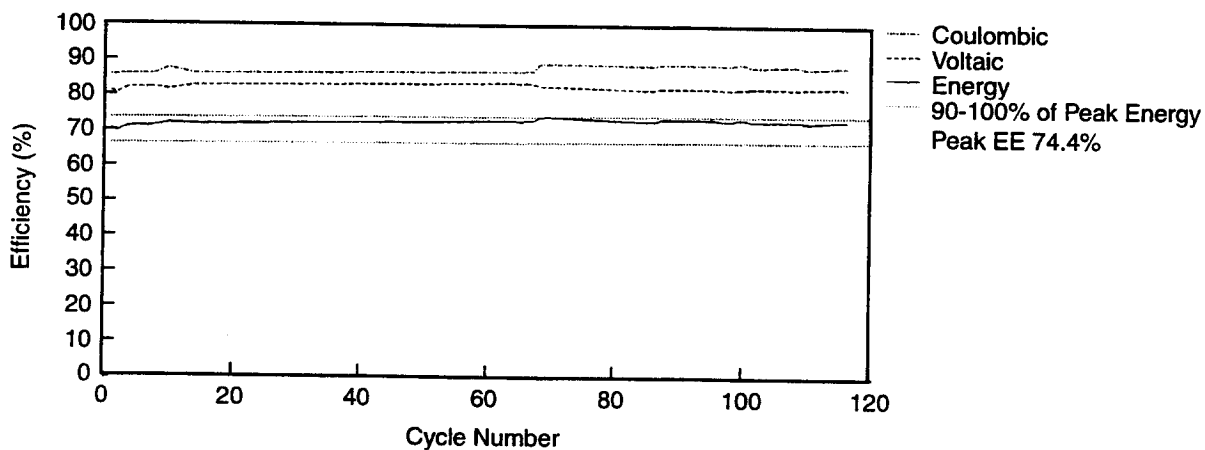


Figure 5-2. Stack V1-54 baseline cycle efficiencies.

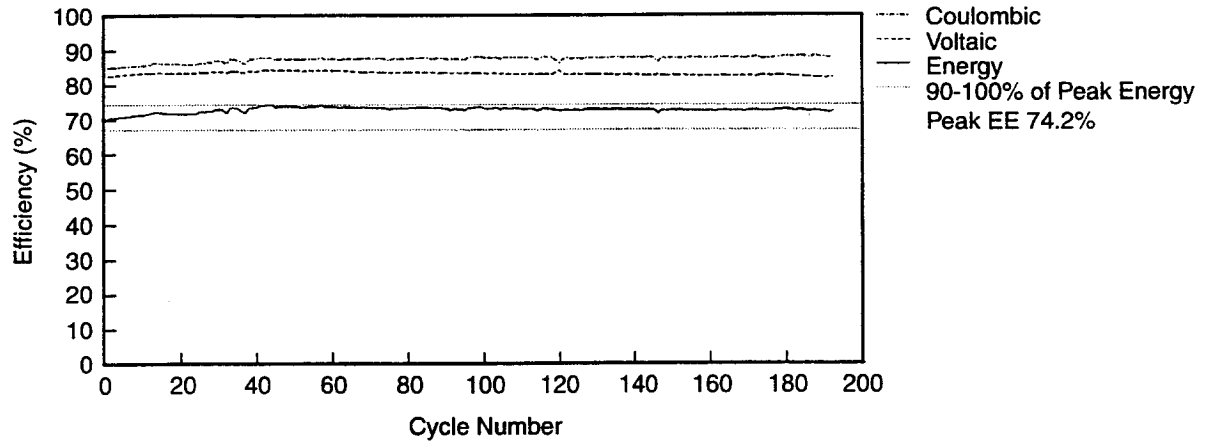


Figure 5-3. Stack V1-55 baseline cycle efficiencies.

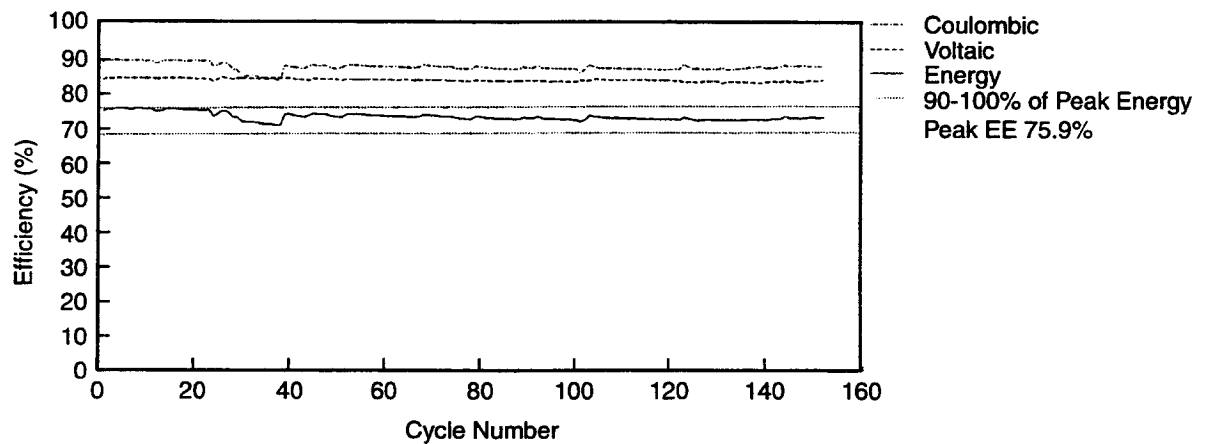


Figure 5-4. Stack V1-57 (SNL 518) baseline cycle efficiencies.

Large Cell Stacks

Seven large, 50-cell stacks were produced during this phase of the project. All seven had satisfactory vibration welds. Two were delivered to SNL as Battery SNL526. Two others were found to have slight seeps at stud holes. Batteries with any kind of electrolyte loss are not considered satisfactory, but the seeps were mostly a cosmetic problem and therefore the cell stacks were cycled to collect operating data. Two of the cell stacks suffered a rapid decline in efficiency. When torn down, the electrode carbon plastic was found to have been incorrectly installed; it was rotated 90° from the normal position. This would lead to a poorly distributed electrolyte flow. The separators were found to be highly degraded and brittle, and some contamination was evident in the electrolyte because of the introduction of a foreign object into the catholyte reservoir.

One cell stack, VL-14, was cycled 27 times and torn down while still operating acceptably so that plating quality could be inspected. The efficiency values for VL-14 are shown in Figure 5-5, and an example of a voltage profile for a baseline cycle is shown in Figure 5-6. Stack VL-16 was cut apart to learn whether an internal weld had failed and thus triggered the seep at the stud hole.

Table 5-2 summarizes life-cycle information on the large stacks including the date when they were built and the total number of cycles through the end of Phase 1.

Table 5-2. Large V-Design Batteries

Stack Date	Total Cycles	Comments
VL-14 07/26/91	107	Taken down to study plating
VL-15 10/17/91	65	Slight seep at stud
VL-16 10/22/91	19	Slight seep at stud
VL-17 10/22/91	13	Falling efficiency, orientation, contaminated
VL-18 11/20/91	13	Falling efficiency, orientation, contaminated
VL-19 01/10/92	*	SNL526
VL-20 01/15/92	*	SNL526

* Tested at Sandia National Laboratories

No-strip Cycling

Laboratory batteries are often stripped, or brought to a completely zero state of charge, following a discharge by shorting the positive terminal to the negative for an extended period. This can be seen in Figure 5-6 as the low-voltage portion of the graph above 500 minutes. Stripping ensures that zinc is deposited on a fresh surface in the next cycle, rather than on top of what could possibly be nonuniform zinc deposits remaining from previous cycles. It also simplifies the data collection procedure for the zinc/bromine battery. Although it is a simple and convenient procedure for lab batteries, stripping will not necessarily be easy or possible to perform on every cycle in commercial applications. For example, a load-leveling battery may be required to operate for at least six cycles without stripping because the typical electrical utility would be able to fully strip the batteries only during a weekend. These considerations have prompted investigations of multiple charge/discharge cycling without stripping.

Efficiency actually increases when a zinc/bromine battery is operated without stripping the last remaining zinc from the electrode after the battery has discharged. The average coulombic efficiency of no-strip cycles is initially higher because a portion of the amp-hours normally lost to stripping is retained in the battery. After a number of cycles, however, the coulombic efficiency will decline, as shown in Figure 5-7. For batteries built before V1-59, this decline occurs after three or four no-strip cycles. Battery V1-59 and later batteries were built with an improved electrolyte flow diverter pattern, and the coulombic efficiency decline is less and occurs after more cycles. Within a set of no-strip cycles, this efficiency loss is exhibited as decreasing capacity. Each cycle discharges fewer watt-hours than the previous cycle. A summary of the efficiency values for all of the no-strip tests is given in Table 5-3.

In Table 5-3, the three efficiencies are calculated as before, but in this table, they are calculated from data taken over the whole set of cycles. The transport inefficiency is the percent of the amp-hours charged that remain in the battery after the discharge is terminated at the cutoff voltage, which is one volt per cell. The values of the coulombic efficiency and the two inefficiencies sum to 100%.

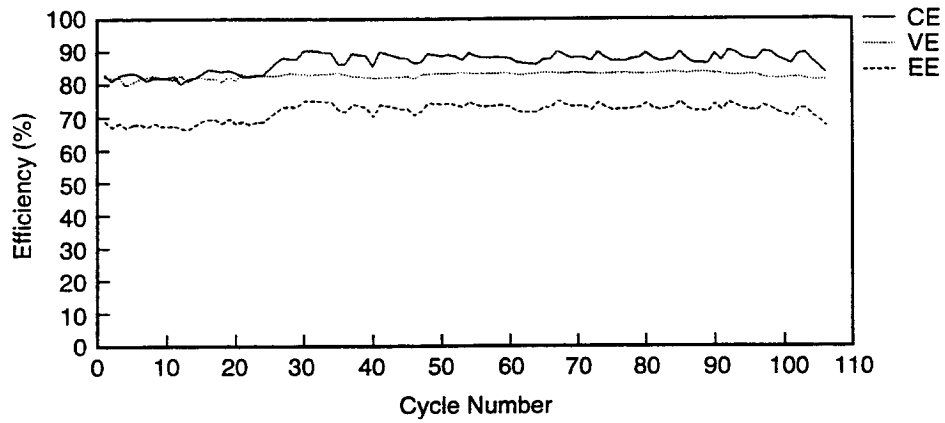


Figure 5-5. Stack VL-14 baseline cycle efficiencies.

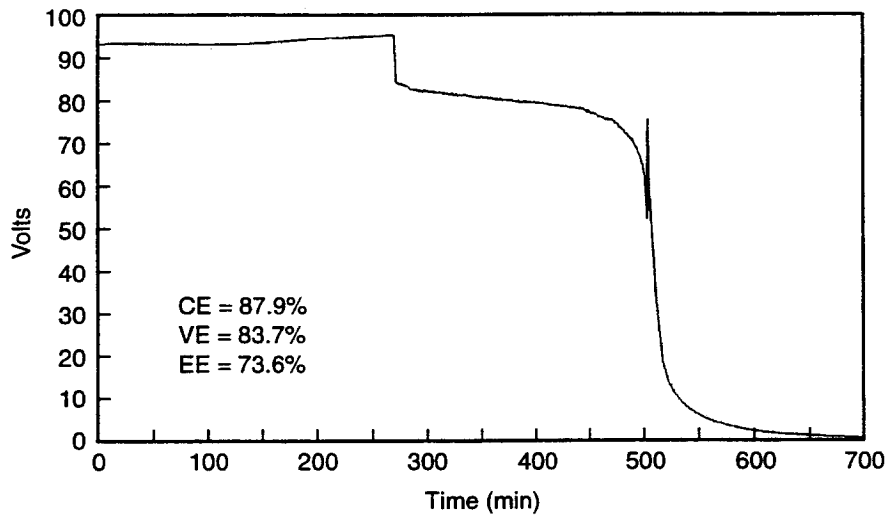


Figure 5-6. Voltage profile of Stack VL-14 for a typical baseline cycle.

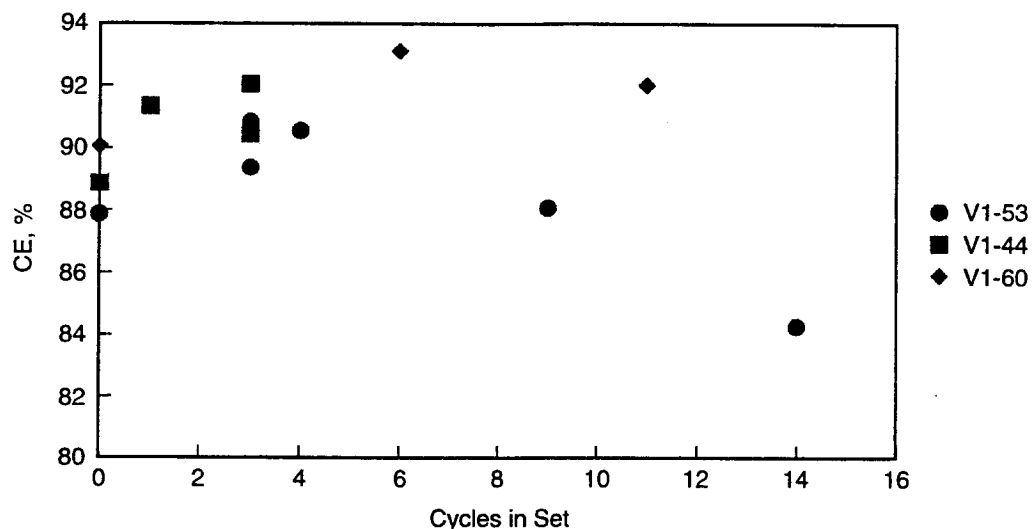


Figure 5-7. Coulombic efficiencies for each set of no-strip cycles.

Table 5-3. Averages of Sets of No-strip Cycles

	Coulombic Efficiency (%)	Voltaic Efficiency (%)	Energy Efficiency (%)	Transport Inefficiency (%)	Residual Inefficiency (%)
V1-44					
Baseline (No. 2,5,10)	88.9	82.9	73.7	6.1	5.0
One cycle (No. 3)	91.4	83.0	75.9	5.9	2.7
Three cycles (No. 6-8)	90.5	82.8	74.9	6.6	1.9
Three cycles (No. 12-14)	92.1	82.7	76.2	5.4	2.4
V1-53					
Baseline (No. 28-31)	87.9	84.4	74.2	7.6	4.4
Baseline (No. 51-55)	87.8	83.9	73.7	7.5	4.7
Three cycles (No. 21-24)	90.6	84.6	76.7	7.1	2.4
Three cycles (No. 47-50)	90.9	84.0	76.4	5.8	3.3
Four cycles (No. 15-19)	90.6	84.6	76.7	7.1	2.4
Nine cycles (No. 56-65)	88.1	85.2	75.0	8.9	3.0
Fourteen cycles (No. 72-86)	84.3	83.0	69.9	12.5	3.1
V1-60					
Baseline (No. 11-14)	90.1	85.9	77.4	5.9	4.0
Six cycles (No. 15-21)	93.2	85.6	79.8	5.1	1.7
Eleven cycles (No. 43-54)	92.1	85.5	78.7	5.8	2.2

Table 5-4. Stand-loss Results
V1-44 – 100% State of Charge (Per = Periodic)

	Pumps/ Second Phase	Coulombic Efficiency (%)	Voltaic Efficiency (%)	Energy Efficiency (%)	Transport Efficiency (%)	Residual Efficiency (%)
Baseline						
Cycle 36	no stand	87.4	82.3	71.9	8.6	4.1
Half-Hour Stand						
Cycle 61	On/Open	87.2	82.4	71.8	8.4	4.5
Cycle 62	Off/Closed	87.2	82.3	71.7	8.5	4.3
One-Hour Stand						
Cycle 37	Per/Closed	86.3	82.4	71.1	8.7	5.1
Cycle 38	Off/Closed	85.3	82.0	69.9	8.1	6.6
Cycle 39	On/Open	86.3	82.6	71.3	8.6	5.2
Two-Hour Stand						
Cycle 44	On/Closed	84.9	82.7	70.3	10.0	5.1
Cycle 45	Per/Closed	86.5	82.2	71.1	9.3	4.1
Cycle 46	Per/Closed	86.2	82.4	71.0	8.7	5.2
Four-Hour Stand						
Cycle 50	Per/Closed	85.4	82.2	70.2	10.1	4.5
Cycle 51	On/Closed	82.5	82.1	67.8	12.0	5.6
Six-Hour Stand						
Cycle 53	Per/Closed	83.1	82.1	68.2	11.3	5.6
Cycle 54	On/Open	79.9	81.9	65.4	13.0	7.2
Cycle 58	On/Closed	80.5	81.8	65.9	13.2	6.3
Baseline						
Cycle 90	No Stand	87.7	81.4	71.4	6.2	6.1
Six-Hour Stand						
Cycle 93	Per/Closed	85.0	81.1	68.9	9.7	5.3
Eight-Hour Stand						
Cycle 95	Per/Closed	83.2	80.8	67.3	10.9	5.9
Cycle 97	Per/Closed	84.2	80.7	68.0	9.9	5.9

The most significant evaluation of the stand loss of a battery system is determining the amount of energy lost and the rate at which it is lost. The results from the tests of Battery V1-44 have been evaluated in terms of the watt-hour capacity lost as compared to a baseline discharge. In this test, the battery is held for a predetermined time at full charge. The second-phase valve is closed, and the electrolyte is circulated periodically. The results indicate a roughly linear one-percent-per-hour loss in capacity, as shown in Figure 5-9. At some point, the capacity loss must level out to a constant value because most of the bromine in the stack will have been exhausted.

Two special tests were done to see if the energy lost while standing could be limited. Theoretically, if a

discharge precedes the stand period the amount of bromine in the stack would be taken to nearly zero, and the following diffusion loss should also be lower. In the first test, the battery was discharged at a decreasing current so that almost all of the bromine active material in the stack was consumed. The battery then stood for 15.5 hours before it was discharged. As can be seen in Figure 5-10, the amp-hour loss was only about 1% above that of a baseline discharge. However, because much of the energy in the first discharge period was removed at a low voltage (average = 3.7 V), the amount of energy recovered was low. That is why the energy loss shown in Figure 5-9 for the 15.5-hour stand test is high.

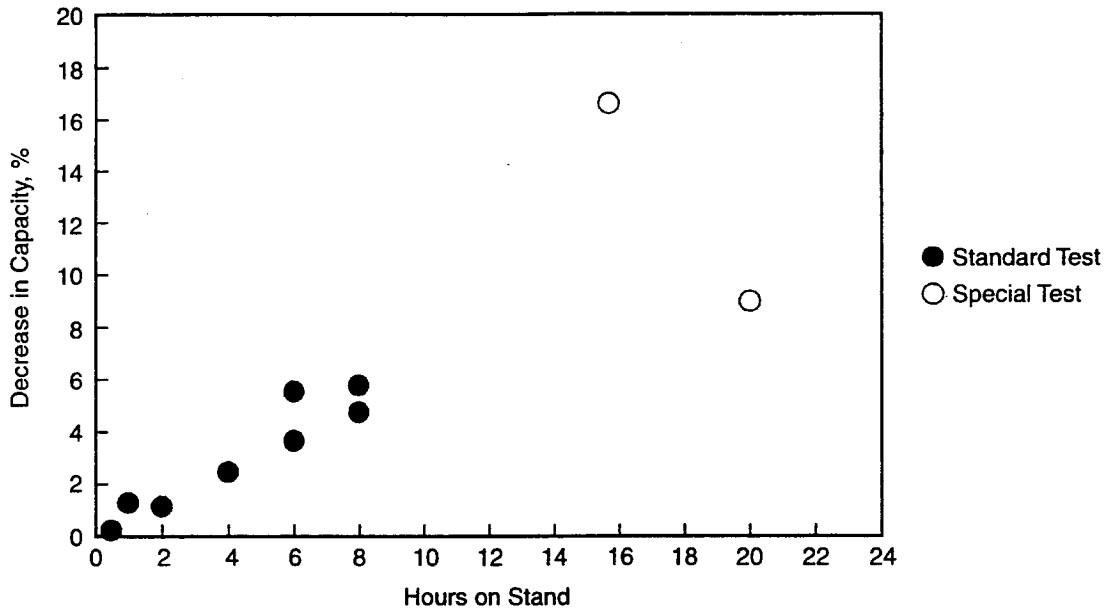


Figure 5-9. Battery V1-44 stand loss at full charge—watt-hour loss compared to baseline cycles.

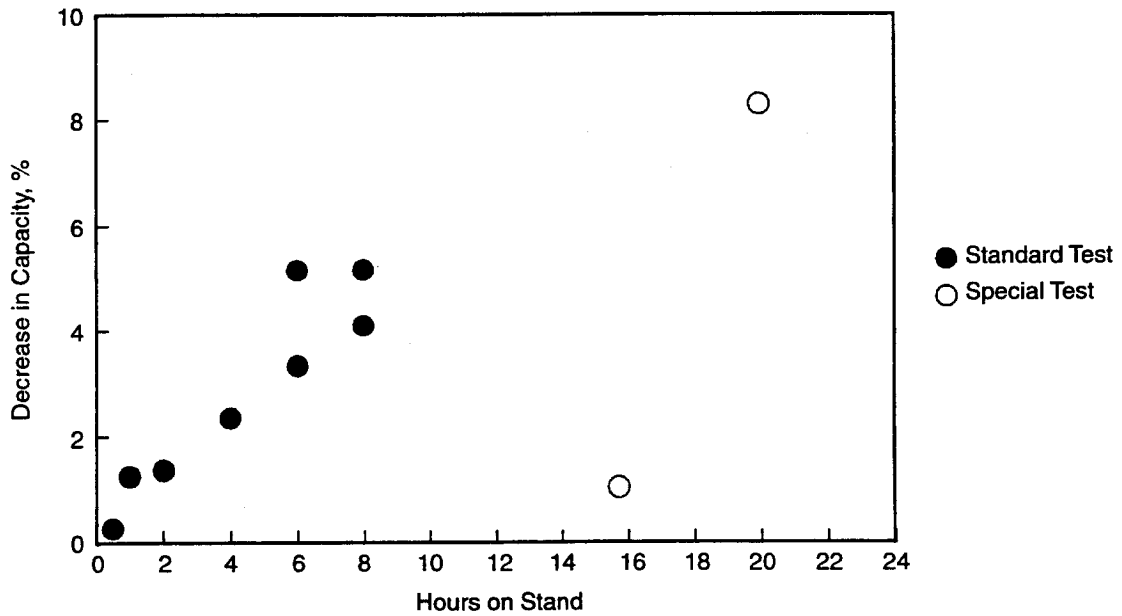


Figure 5-10. Battery V1-44 stand loss at full charge—amp-hour loss compared to baseline cycles.

In the second special test, the battery was discharged at the C/3 rate until the voltage fell to the normal cut-off value (average = 12.8 V). However, so few amp-hours were taken out by the special discharge that the amp-hours lost to diffusion during the shutdown remained high, as seen in Figure 5-10 at 20 hours of stand. The energy loss shown in Figure 5-9 was close to what would be predicted from an extrapolation of the results of the standard shutdown tests.

There should be a natural limit to the amount of stand loss that can be expected because once the bromine in the stack has been consumed, all reactions stop. Testing will be continued to find this level of stand loss.

Zinc Loading

A study was performed to extend the zinc loading upper limit and to evaluate the effect of zinc loading on the performance of the zinc/bromine battery using standard load-leveling electrolyte. All the trials were carried out at constant current using the baseline cycle current density (20 mA/cm²), zinc bromide utilization (80%), and temperature (30°C).

The zinc loading study began at 45 mAh/cm² and progressed in increments of 5 mAh/cm² to a loading of 130 mAh/cm² (the standard loading in a baseline cycle is 90 mAh/cm²). The results have indicated that there is virtually no change in the coulombic, voltaic, and energy efficiencies up to a loading of 115 mAh/cm². The results achieved to date with battery V1-54 are shown in Figure 5-11. The performance of the test battery, V1-54, has declined slightly, but no more than seen in other long-term tests.

Temperature Effect

To establish the temperature range in which performance is optimized with the load-leveling electrolyte, battery operation was studied in the range of 21°C to 45°C. The temperature during the test was controlled to within 1°C.

The results, shown in Figure 5-12, indicate that the energy efficiency is highest at 30°C and decreases by 3% when the temperature is raised to 45°C. The effect of temperature on efficiency is influenced by two factors: electrolyte resistance and bromine diffusion rate. At higher operating temperatures, the electrolyte

resistivity is lower, and this improves the voltaic efficiency. However, the coulombic efficiency decreases as the temperature is raised because the rate of bromine transport across the separator is also increased. The maximum coulombic efficiency was achieved at 21°C, the lowest temperature. Between 21°C and 45°C, the coulombic performance decreased by 6.5%.

Fast-strip Cycling

In many zinc/bromine battery applications, there may be only limited opportunities for stripping the remaining zinc from the negative electrode. Therefore, it is important to strip the battery as quickly as possible. One way to do this is to mix the two electrolytes when the stripping process begins, so that the remaining bromine can react directly with the plated zinc.

Two batteries were fast-stripped by switching the electrolytes at the beginning of the strip period. Two methods were used to determine the strip time. In the first, the time until the total amp-hours no longer changed (0.1-Ah increments) was measured; in the second, the time until the voltage fell below 0.01 V/cell was recorded. In general, the strip times determined by voltage reading were shorter, but all except for the V1-53 voltage times were rather scattered. The strip times listed in Table 5-5 show that in each case, the fast-strip method was more effective than the conventional method. The test demonstrates that the strip period can be limited to 1.5 to 2.0 hours by admitting bromine-containing electrolyte to the zinc electrodes.

Table 5-5. Strip Times

Battery/Cycle	To ΔAh = 0 Minutes	To V<0.01 Minutes
V1-50/23	386	190
V1-50/24	346	282
V1-50/25*	95	85
V1-50/26	160	125
V1-53/29	206	135
V1-53/30	176	136
V1-53/31	569	136
V1-53/32*	131	96
V1-53/33	333	136

* Fast-Strip Test

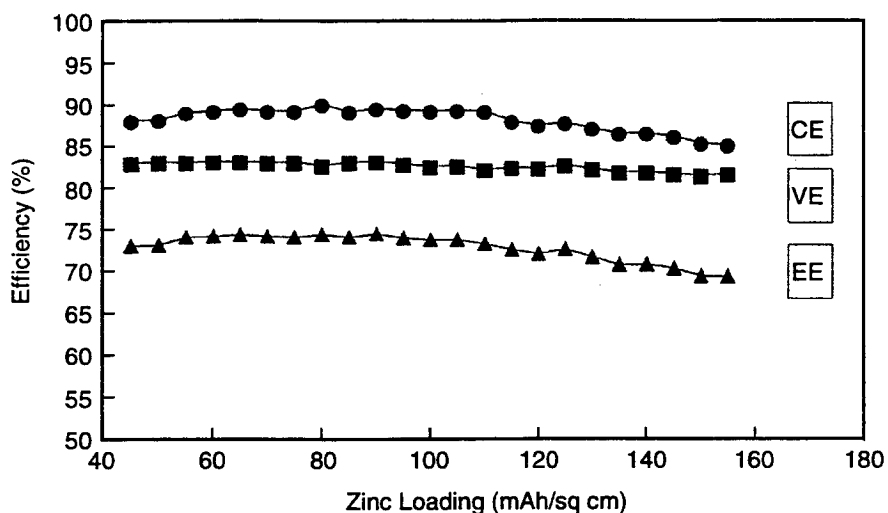


Figure 5-11. Zinc loading study (Battery V1-54).

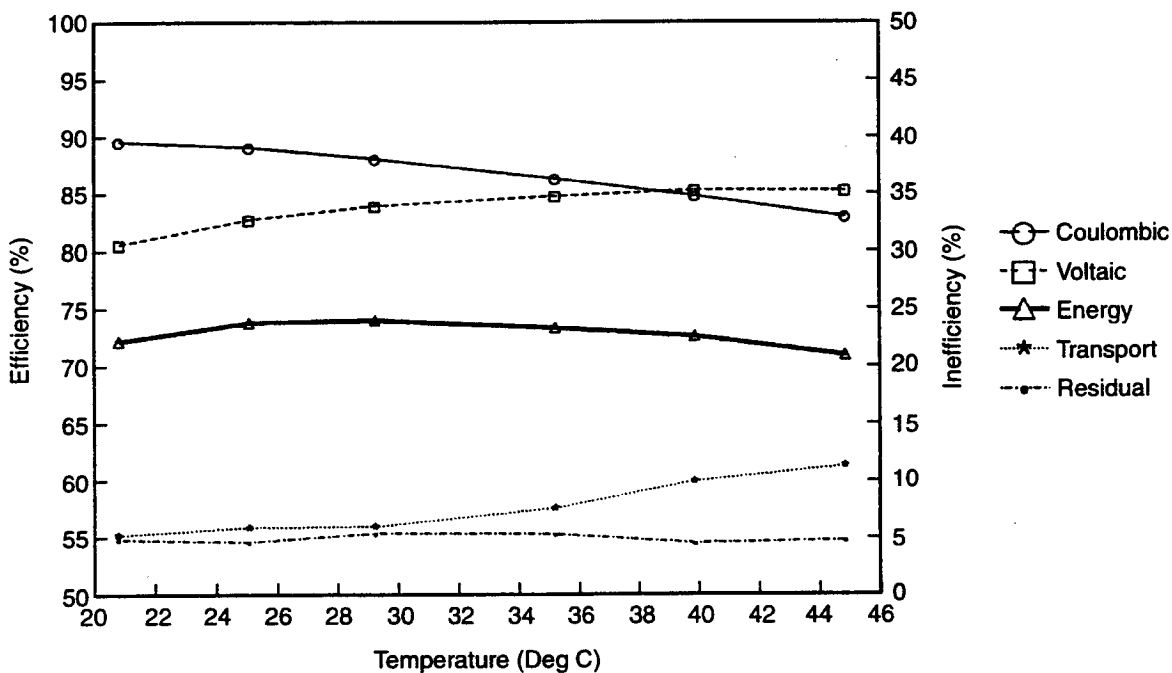


Figure 5-12. Temperature effect study—efficiency vs. operating temperature (Battery V1-50).

Experimental Separator Battery Test

Battery V1-51 was built with an experimental separator provided by a vendor. After peaking at 72.6% energy efficiency during the first week of operation, the battery returned increasingly lower efficiencies. By Cycle 40, the energy efficiency fell to 66.3%. A calculation using the mass and energy spreadsheet indicated that the losses were occurring in bromine transport and residual capacity. The calculated values are listed in Table 5-6.

Table 5-6. V1-51 Performance – Energy Losses

	Cycle 4	Cycle 41
Efficiency		
Coulombic	84.6%	79.4%
Voltaic	85.5%	83.5%
Energy	72.4%	66.3%
Energy Loss by Categories		
Resistance, Wh	225	218
Overtoltage, Wh	34	33
Shunt Current, Wh	<1	<1
Diffusion, Wh	152	199
Residual, Wh	81	114
Total, Wh	492	564

The energy lost to bromine diffusion showed the largest increase. This may also indicate some partial dendrite penetration or other deterioration of the separator. Surprisingly, the energy lost to resistance decreased slightly, even though the voltaic efficiency also decreased. The voltaic efficiency drop would occur if the average voltage on discharge decreased. This can happen if the discharge ends early because some of the active material has been lost. An increase in residual loss in this case probably indicates that the zinc that reacted with the bromine was not uniformly distributed on the anode surface.

Shunt-current Protection

Shunt-current Protection Current

In the present V-design, shunt-current protection (SCP) is provided by a set of electrodes and tunnels through the stack. The current in the tunnels sets up a

potential field that matches the potential expected from the shunt current in the electrolyte channels and thus removes the driving force for shunt currents in the channel. Battery V1-39 was fitted with tunnels in the frames and four SCP electrodes.

The tunnel current required to stop shunt currents was calculated using a published method.¹ The minimum tunnel current needed is much smaller than the current actually seen at the SCP electrodes. The tunnel current is set by a combination of the stack voltage, the size of the resistors that connect the SCP electrodes, the resistance of the electrolyte, and the diameter of the tunnels. Because the diameter of the tunnels is relatively large in the present 8-cell stacks, the tunnel current is expected to be larger than the minimum required to block the shunt current. The minimum tunnel currents, based on a predicted tunnel diameter of 0.04 cm, was calculated at 2 mA. The expected tunnel current, based on the 0.2-cm diameter tunnels actually used, was calculated at 48 mA.

The currents measured at the SCP electrodes on Battery V1-39 were typically about 400 mA, but when the opposing electrode was disconnected, the current dropped by about 110 mA. Assuming that this change in the current was the true tunnel current, the remaining current must be diverting to the main electrodes. There are two tunnels connected to each SCP electrode, so assuming an equal split of the tunnel current, each tunnel had about 55 mA. This is a surprisingly good match to the 48-mA tunnel current calculated in the previous paragraph.

The results indicate that the tunnel holes should theoretically be much smaller to approach the minimum tunnel current. However, the use of small holes could lead to difficulties because small holes are likely to plug easily with either carbon particles or second-phase particles.

Further, the experiments indicated that the individual SCP electrode currents were larger than expected, and must have been composed of more than just tunnel currents. Large currents subtract from the battery efficiency and overwork the SCP surfaces.

¹ P. Grimes, R. Bellows, and M. Zahn. 1984. "Shunt Current Control in Electrochemical Systems Theoretical Analysis," p. 259 in *Electrochemical Cell Design*, Ralph E. White, Ed., Plenum Press, New York.

Shunt Currents

Under ideal conditions, it is possible to measure the equivalent shunt current in a large stack by comparing the coulombic efficiency with that of a smaller battery where the shunt currents are negligible. In this way, the average equivalent shunt current for Batteries VL-15 and VL-16 was found to be about 0.087 A, which is very close to the values estimated by model calculations.

If all other factors are equal, the difference between the coulombic efficiency of a stack with a large number of cells and that of a stack with a small number is caused only by the shunt current. Therefore, this difference in coulombic efficiency should allow the shunt current to be calculated for a cycle. The average coulombic efficiency for Batteries VL-15 and VL-16 during Cycles 1–10 was 89.5% with a standard deviation (sd) of 0.3%. For 8-cell stacks V1-60 and V1-62 during Cycles 8-14 and 1-10 respectively, the coulombic efficiencies were 90.2% sd 0.1% and 90.3% sd 0.2%. Therefore the coulombic efficiency of VL-15 and VL-16 was lowered by 0.7%. The typical charge for VL-15 and VL-16 was 104.75 Ah; 0.7% of this is 0.73 Ah. The total cycle time was 8.352 hr, which means that the shunt current process diverted 0.087 A away from useful work.

Shunt currents were also predicted by two models. The average shunt current for a 50-cell load-leveling stack had been approximated by a shunt current model as being 0.115 A.² The zinc/bromine battery empirical model predicted 1.66-Ah loss per cycle, which is equal to 0.199-A equivalent shunt current.

In addition to the direct energy lost when shunt currents redirect a portion of the internal currents away from the working electrodes, shunt currents can also contribute to residual losses.³ While the highest individual shunt currents are at the terminal electrodes, the highest total redirected current occurs at the middle cells of the stack. On charge, that means there is less zinc plating in middle cells. On discharge, however, the current at the main electrodes is actually higher because of shunt currents. Therefore, the zinc depletes more rapidly in the middle cells. Because there was less zinc in the middle cells to begin with, zinc depletion occurs there earlier, and the battery voltage drops.

Shunt current calculations indicate that for Battery SNL514 (50 cells) Cycle 27, the shunt currents caused a direct loss of about 1.2% of the amp-hours charged by increasing the residual inefficiency. When the battery was charging at 23.5 A, the current in the middle cell was actually 23.3 A; then during discharge, the battery current was 24.2 A, but the middle cell current was 24.3 A. This resulted in 0.94 Ah less plating than in a comparable 8-cell stack, and the plating was removed 3.4 minutes earlier than it would have been had the battery been an 8-cell stack. The small deviation indicates that the effect was not especially important in that cycle, but the effect should be considered for other cycles and other stacks where it may become significant.

² E.A. Kaminski and R.F. Savinell. 1983. "A Technique for Calculating Shunt Current Leakage and Cell Currents in Bipolar Stacks Having Divided or Undivided Cells," *J. Electrochem. Society*. Vol. 130, p. 1103.

³ K. Kanari et al. 1991. "Numerical Analysis of Shunt Current in Zinc-Bromine Battery," *Denki Kagaku oyobi Kogyo Butsuri Kagaku* 59(3). p. 237.

Intentionally Left Blank

6. Summary/Conclusions

In Phase 1 of the contract, the state of the art for zinc/bromine battery technology has been improved. The unique, hermetically sealed cell stack has been shown to be leak-free when properly designed and manufactured. The stack energy efficiency results are 75% and higher for the most recently built batteries. Several life tests of 8-cell battery stacks have achieved more than 100 cycles with only minor performance degradation. One stack has achieved more than 250 cycles. All of the life-cycle tests will continue after the end of Phase 1. Work is under way to identify the causes of the efficiency decline and to retain high performance.

Supplemental tests of battery performance under no-strip cycling regimes have shown that the battery is capable of performing more than a dozen cycles without stripping the zinc. With uniform electrolyte flow, as in the most recently built stacks, the energy efficiency is actually improved because fewer watt-hours are lost to unreacted zinc and bromine left in the battery at the end of the cycles. Stand losses were found to be initially about 0.66% of the energy capacity per hour. Although this is a relatively high rate, the loss is limited to the bromine that is in the cell stack. In future tests, the maximum loss will be measured, and work will be done to lower the stand loss rate. Although in the present baseline battery cycles, the stack is charged to 90 mAh/cm², the loading was tested to 115 mAh/cm² without any apparent negative effects. The battery was found to operate at

peak energy efficiency at 30°C. Higher losses to resistance occurred at a lower temperature, and bromine transport increased at a higher temperature. The ability to accelerate the stripping process to as short a time as 1.5 hours was demonstrated.

A welding study and a modeling study of the battery operation were used to prepare for the next stage in the load-leveling battery design. The optimum weld-bead size, materials, and welding parameters were developed for the production of a new cell stack. The battery model was improved to the point where it not only can predict trends but now closely matches the observed results of charge/discharge cycles. Initial work on battery recycling and safety suggest that these will be positive factors in the adoption of the zinc/bromine technology.

In this phase of the contract, the basic design and performance of the zinc/bromine battery has been demonstrated to be appropriate for load-leveling use. A number of the tests to explore the operating parameters of the zinc/bromine battery are ongoing, as are investigations into improved zinc plating and bromine electrode surfaces. The results of this continuing work will only improve the overall acceptability of the battery for load-leveling applications. In the next phase of this program, the improved zinc/bromine technology will be scaled up to a size appropriate for a submodule of a 100-kWh battery suitable for use in a load-leveling facility.

Intentionally Left Blank